WIRELESS PULSE OXIMETER

A Major Qualifying Project Report

submitted to the Faculty

of the

WORCESTER POLYTECHNIC INSTITUTE

in partial fulfillment of the requirements for the

Degree of Bachelor of Science

by

_____

Joseph Bailey

_____

Michael Fecteau

_____

Noah L. Pendleton

Date: April 24, 2008

Approved:

_____

Professor Hossein Hakim, Advisor

ABSTRACT

The goal of this project was to create a prototype wireless pulse oximeter patient monitoring device that was low cost and had good battery life. The final design combined a low-power analog sensor circuit with a software DSP system and a low-power wireless transceiver. The prototype device connects to a Windows PC via USB. The final product fulfilled the low-power and low-cost objectives of the project.

TABLE OF CONTENTS

LIST OF FIGURES

LIST OF TABLES

1 INTRODUCTION

Oxygen gas is necessary for human life. It is integral for countless biological processes. The transport of oxygen throughout the human body is performed by the circulatory system, and more specifically, hemoglobin in red blood cells. Critical medical information can be obtained by measuring the amount of oxygen in blood, as a percentage of the maximum capacity.

Pulse oximetry has become a standard prcedure for the measurement of blood-oxygen saturation in the hospital operating room and recovery room. Oximetry shortens the time passed before the detection of hypoxemia, or deficiency of oxygen. Hypoxemic events have been documented in the critically ill during invasive or diagnostic procedures, and during movement from one location to another. Significant hypoxemic events are also common during cardiac catheterization, or inserting a catheter into a chamber or vessel of a patient's heart. Pulse oximetry also provides an early warning of oxygen ventilator malfunction. Finally, pulse oximetry provides an important function in the intensive care unit, as an early warning system for patient emergencies. Otherwise unsuspected episodes of low blood oxygen can be detected accurately and quickly. Monitoring of a patient through wireless telemetry can be done to view data from numerous remote patients on a single display. [1]

In addition, many screening devices for sleep apnea use pulse oximetry as its most important parameter. [2] By recording oxygen saturation and pulse readings during sleep, pulse oximetry can be an effective and low-cost screening tool that may be used away from the hospital. With the information being easily analyzed and viewed on a computer, it can be a worthwhile, objective view. [3]

Wireless pulse oximetry adds many advantages to the traditional wired units. They are more convenient for the patient to use, and can be more comfortable; wireless units don't need to be reconnected each time the patient is moved. Many wireless units are already available from several manufacturers. This product developed in this project provides several advantages over existing models, primarily adding a longer battery life and a low unit cost.

In determining the improvements this design will exhibit, it is important to review existing products in this field. This will clarify the specific advantages this design can provide over previous devices.

1.1 PRIOR ART

There are many models and brands of pulse oximeters. A sampling based on popularity and features was chosen. The models described cover the full gamut of possible feature sets, from completely wired and stationary units, to highly portable disaster-relief and triage models, to Bluetooth-compatible wireless units.

Avant 9700

Figure 1: Avant 9700 by Nonin

The Avant 9700 is an industry leader pulse oximeter. The sensor is connected to the display via a wire. Oxygen saturation, pulse, and plethysmograph are displayed in bright LED displays. The unit can be either AC powered or battery powered.[4]

GE TruSat

Figure 2: GE TruSat

The GE TruSat pulse oximeter is a durable model that displays oxygen saturation and pulse. The LCD display is backlit for easy viewing. It can either be powered by AC or battery power.[5]

Avant 4000

Figure 3: Avant 4000 by Nonin

The Avant 4000 system is the first Bluetooth pulse oximeter. The wireless communication is point to point, so this oximeter uses Bluetooth as a cable replacement. Oxygen saturation and pulse rate are displayed in bright LED displays.[6]

3100 WristOx and SPO 7500

Figure 4: Nonin WristOx

Figure 5: SPO 7500

Nonin's WristOx[7] and SPO medical's SPO 7500[8] are both wrist worn devices that are intended for sleep and long term studies. They store periodic readings in memory that can be downloaded to a PC for viewing and analysis. Both display current data on a small LCD display attached to the wrist. The SPO 7500 is unique because it uses a reflectance sensor, as opposed to transmission.

Philips Intellivue System

Figure 6: Philips Intellivue Transmitter

The Intellivue system is a complete cellular network. A patient wears a device that takes electrocardiogram and pulse oximetry readings. This device then connects to a hospital network via wireless access points. It is therefore only used in a hospital environment because there is no ad hoc networking capability. The telemetry operates at 1.4GHz and is based on the DECT standard for European cordless phones. This offers adaptive frequency hopping which increases the reliability of the communication, as well as limits interfering with other telemetry. If a certain frequency band is in use, the radio will not communicate on that band.[9]

Table 1: Pulse Oximeter Model Comparison

Model	Batteries/Power	Battery Life	Telemetry Standard	Telemetry Range	Pleth Wave	Accuracy	Cost
Avant 4000 (Nonin)[6]	Two AA batteries Tx, AC/Rech Bat display	>120 hours Tx, 18 hours display	Point to Point BlueTooth, 2.4GHz	10m	No	2% SPO2, 3% Pulse	$1,650
Nonin WristOx[7]	Two 1.5V N-cell	24 hours	NA	NA	No	2% SPO2, 3% Pulse	$725
Avant 9700 (Nonin)[4]	AC/Rech Bat	12 hours	NA	NA	Yes	2% SPO2, 3% Pulse	$1,995
SPO 7500[8]	3.6V Lithium	300 hours	NA	NA	No	2% SPO2, 3% Pulse	$499
GE TruSat[5]	AC/Rech Bat	20 hours	NA	NA	No	2% SPO2, 2% Pulse	$1,895
Philips Intellivue[9] [10]	Two AA batteries	17 hours	DECT, 1.4GHz	35m	No	2% SPO2, 3% Pulse	*Unknown, units bought as a cellular infrastructure*

1.2 WIRELESS NETWORKS

It is relevant to assess the role of wireless networks, in order to determine in which ways a certain type of wireless pulse oximeter can be superior to other types of the same device. This section reviews the use of wireless networks in medical settings. The information covered here should provide an appropriate context for the design decisions made regarding the wireless function of the project.

Wireless Equipment in Hospitals

Wireless technologies have been maturing and expanding over the last few decades, most notably in the form of wireless telephones or computer networks. Wireless devices have invaded many other sectors of commerce and industry, from RFID tags replacing scan barcodes to long-range Wireless Area Networks connecting computer users over longer and longer distances. These technologies are being depended on more and more for critical tasks, in military, scientific, and most important to this project, medical applications[11].

Figure 7: LifeSync Corporation's wireless EKG (electrocardiogram)

The primary use for wireless technology in a medical environment is to aid in patient monitoring. This can range from simply providing a way to track the location of patients, as in RFID tag systems, to advanced EKG and remote status viewing of multiple patient vitals. The advantages to making these systems wireless are twofold[12]:

1. allows for mobility of patient without disconnecting monitoring equipment

2. allows medical staff to remotely keep track of patients' well-being, including remotely informing staff of emergency conditions for a patient

The other great benefit of wireless medical equipment, specifically wireless patient monitoring, is that patient information can be continuously collected and deposited in hospital data banks, providing an excellent record of a patient's medical status regardless of whether the patient is stationary or ambulatory, so long as the patient's wireless monitoring gear is within range of hospital receivers[13].

Current Wireless Transmitter Methods Used By Wireless Pulse Oximeters

Pulse oximetry measurement is hardly new; the first wired pulse oximeters were released in the late 1980s[14]. More recently, several wireless versions of these finger-clip-style sensors have been appearing. These units have all the advantages of wired pulse oximeters, such as rapid reading acquisition and low-impact status monitoring of patients, combined with the convenience of wireless technology.

Wired pulse oximeters are used in hospitals and other health care facilities to provide doctors with a reading of a patient's SpO_2[*] level and heartrate. They are often used in conjunction with EKG sensors and other status monitors, which display their information along with the pulse oximetry readings, as seen below, on a patient's medical monitoring display:
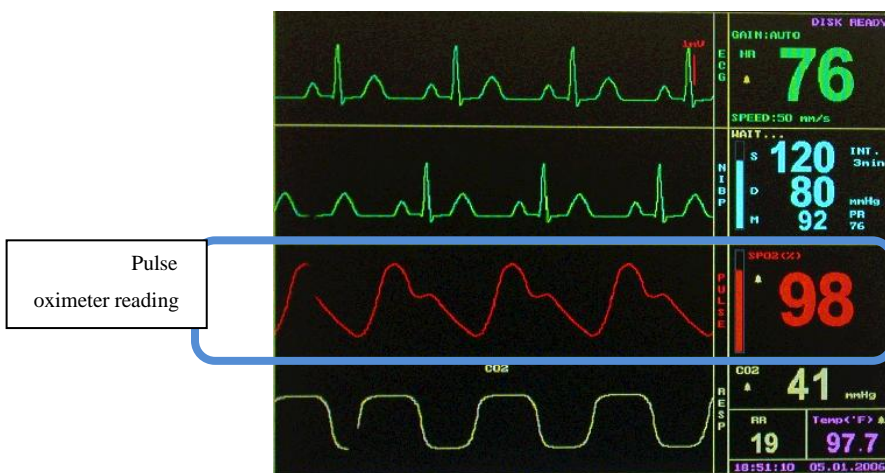
Figure 8: Patient monitoring display, showing an SpO2 reading of 98%[15]

---

[*] Saturation of Peripheral Oxygen

The earliest "wireless" pulse oximeter is the portable-style pulse oximeter. While these units are not truly wireless, as they transfer sensor readings through a wired lead, they are self-contained and very portable. These are especially useful in emergency situations, where equipment is limited and ease-of-use is of high importance. As these devices are self-contained, there is no need for a patient monitoring display as in a hospital situation, so portable-style pulse oximeters are also convenient when a facility needs to monitor SpO_2 on a patient, but has no available external patient status displays.

Figure 9: Nonin all-in-one portable pulse oximeters[16]

This type of pulse oximeter is most useful in triage situations where efficiency is paramount[17]. The downside to these units is that most of even the best products do not record the sensor information for later analysis. Important information is therefore lost, which could affect a doctor's medical decisions for a patient; this kind of information could include a record of an arrhythmic heart beat, for example.

Truly wireless pulse oximeters are available from several medical equipment vendors. One example is Alive Technology's wearable pulse oximeter, pictured below.

Figure 10: AliveTec wrist-style wireless pulse oximeter[18]

Many of the wireless pulse oximeters currently being produced use Bluetooth networking systems, which is the first task group of the IEEE 802.15. There are three advantages to using Bluetooth over other low-power PLAN systems:

1. High frequency-to-noise ratio (up to -104dB receiver sensitivities, and transmission strengths of 23dBm or more)
2. Capable of high data rates, theoretically up to 2.1 Mbit/s (Bluetooth 2.0)
3. Bluetooth technology is present in <u>many</u> cellular phones, PDAs, and notebook computers, making any Bluetooth-enabled device very technologically compatible

Bluetooth is also a very mature technology, with a multitude of chipsets available from many vendors and well-explored transmission and encryption software. However, it shares the downsides of all PLAN systems, which include short-range effectiveness and weakness towards interference, as it shares the 2.4GHz band with the higher-power 802.11 WLAN traffic. Bluetooth also possess a number of additional disadvantages specific towards our needs.

First, Bluetooth transceiver chips are somewhat high-power for this application; up to 190ma during transmission[19], and even with a low duty cycle, current draw is still higher than would be preferred. Second, the protocol stack for Bluetooth transmission is much larger than that of other PLAN systems, and therefore demands a microcontroller with greater memory[20].

Besides Bluetooth, there are other wireless variants within the 802.15 specification that are very applicable to small-area, low-bandwidth uses such as patient monitoring. The IEEE 802.15.4 task group focuses on low-bit-rate WPAN[†], with peak speeds of 100-250 kbps. ZigBee provides an upper-level specification for the 802.15.4 standard, which is targeted towards

---

[†] Wireless Personal-Area Network. Typical transmission distance is only a few meters for these LANs.

applications needing long battery life, secure networking, and a low data rate[21]. The advantages to using a ZigBee-based wireless transmitter include:

1. Very long battery life, with average current draws in the 30mA range for Tx. This current draw is low enough to last almost 100hrs on a single AA battery.
2. Secure data transfer, with 128-bit encryption
3. Simple, integrated architecture using the ZigBee specification
4. ZigBee-compliant hardware is very inexpensive. An entire transceiver solution at quantities of 1000 can cost less than US$5.

Although ZigBee lacks the throughput of even Bluetooth, which is a low-data specification, it certainly has a high enough data rate for an uncomplicated sensor reading; in fact, target applications for ZigBee include wireless sensors and monitors, such as water or gas metering, or medical monitoring, in this case. Also, ZigBee is well suited to Reduced Function Device (RFD) networking, in a simple star-style network opposed to the mesh or cluster-tree network topologies. This is ideal for a group of sensor-transmitter communicating with a single receiver, as in our application.
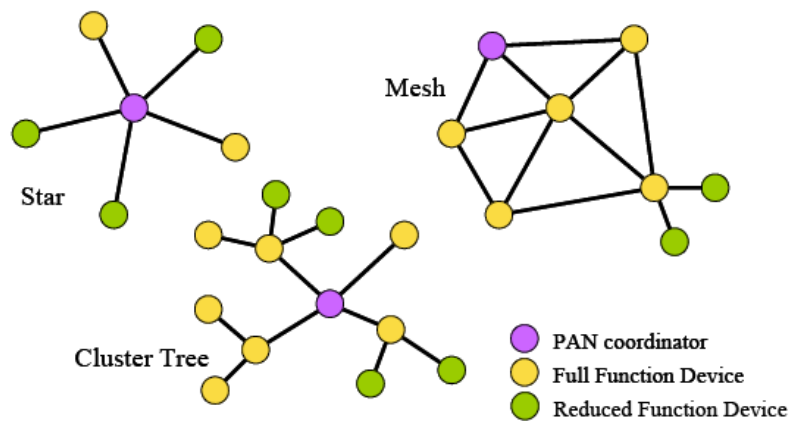
Figure 11: ZigBee network topologies[22]

Overview

Wireless pulse oximeters are new to the market, with only a few companies producing these devices. Most of the current-model wireless pulse oximeters use the Bluetooth transmission specification to communicate sensor readings. There are, however, significant

disadvantages to using the Bluetooth specification for this application, most notably battery life. The ZigBee specification is much more suited to wireless patient monitoring, and although it lacks the cross-integration of Bluetooth, it has the advantages of significantly increased battery life, a simpler yet still secure transmission scheme, and lower system cost than Bluetooth[‡][23]

[‡] System package cost including radio, processor, and memory

2 BACKGROUND

2.1 THEORY

The main operation of a pulse oximeter is the determination of a person's functional oxygen saturation. Arterial oxygen saturation, or S_aO_2, is the percentage of functional arterial hemoglobin that is oxygenated. Functional hemoglobins are a type of hemoglobin that is able to bind with oxygen. Non-functional hemoglobins cannot bind with oxygen. An example of non-functional hemoglobin is carboxyhemoglobin (COHb), which binds easily with carbon monoxide. When a functional hemoglobin binds with four oxygen molecules, it is considered an oxygenated hemoglobin (HbO_2). When it is carrying less than four oxygen molecules, it is considered reduced (Hb). Functional oxygen saturation measured with a pulse oximeter is often called S_pO_2[§] because it is an estimation based peripheral measurements and an assumption that only HbO2 and Hb are present in the blood. The presence of non-functional hemoglobins such as COHb can cause erroneous measurements. Therefore, S_pO_2 is a different measurement than S_aO_2.[24]

$$S_pO_2 = \frac{HbO_2}{Hb + HbO_2}$$

Oxygenated and reduced Hemoglobin differ in their absorption of light, a fact that pulse oximetry exploits to find the relative levels of the two hemoglobins. The most common pulse oximetry uses a red LED and infrared LED to shine light through a person's finger. A light detector is used on the other side of the finger to measure the transmitted red and infrared light.[25]
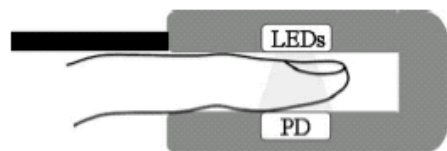
Figure 12: Transmission Type Sensor

[§] S_pO_2, or SpO2, stands for "Saturation of Peripheral Oxygen". It refers to the concentration of oxygen in a patient's periphery; in this case, it is usually measured in a fingertip or earlobe

The red and infrared LEDs are generally pulsed in an alternating fashion, so that one photo-detector can be used to measure the light intensity of both LEDs.

With a known measurement of red and infrared light transmitted through the finger, an estimate of the ratio between oxygenated hemoglobin and reduced hemoglobin can be determined based on extinction (absorption) curves at the various wavelengths of transmitted light. A typical oximeter works with 660nm red light, and 940nm infrared light. At 660nm, reduced hemoglobin absorbs about ten times as much light as does oxygenated.[§]
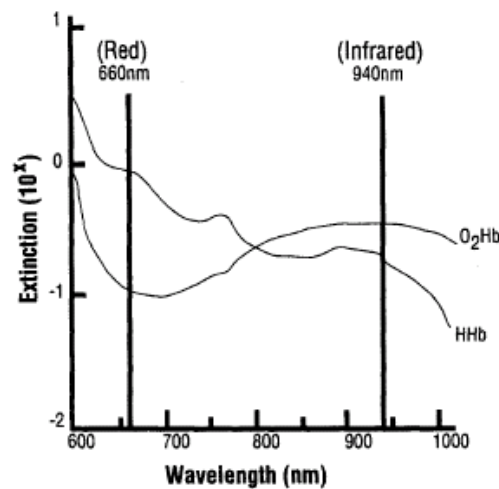
Figure 13: Extinction (absorption) of light from oxygenated and reduced hemoglobin[25]

Because the flow of blood is pulsatile in nature, the transmitted light changes with time. A normal finger has light absorbed from bloodless tissue, venous blood, and arterial blood. The volume of arterial blood changes with pulse, so the absorption of light also changes. The light detector will therefore see a large DC signal representing the residual arterial blood, venous blood, and bloodless tissue. A small portion of the detected signal (~1%), will be an AC signal representing the arterial pulse. Because this is the only AC signal, the arterial portion of the signal can be differentiated. This AC signal is separated with simple filtering and an RMS value can be calculated.[25]
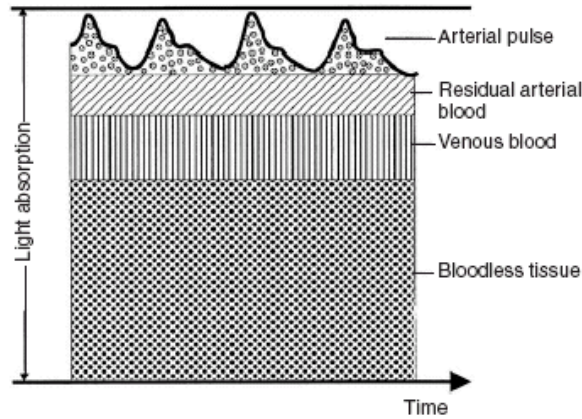
Figure 14: Light Absorption by Tissue Type[25]

An intermediate value, known as the Normalized R ratio, is calculated using these signals.

$$R = \frac{\left(\dfrac{ACrms660nm}{DC660nm}\right)}{\left(\dfrac{ACrms940nm}{DC940nm}\right)}$$

This value represents a ratio of reduced to oxygenated arterial hemoglobin. Using this value, a value of oxygen saturation is calculated based on empirical data.[§]
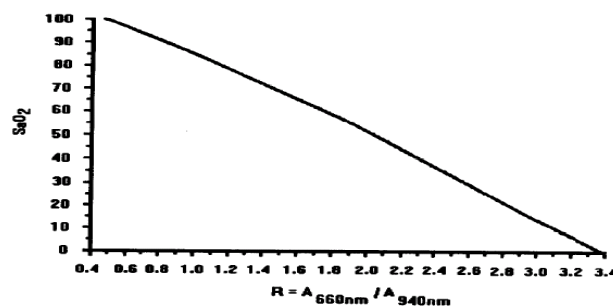
Figure 15: Empirical Oxygen Saturation Curve (vs. R)[26]

This empirical curve can be closely approximated by a linear equation[24]:

$$S_pO_2 = 110 - 25 \times R$$

Readings below 70% are not accurate, but very few if any clinical decisions rely on accuracy below this point[26]. Using the arterial AC signal from either the red or infrared sources, the pulse rate can be determined using simple algorithms such as zero crossing, or an FFT.[25]

2.2 SIGNAL TOPOLOGIES

Design of the pulse oximeter can take a highly analog approach or a highly digital approach. Two prior art designs were compared, looking at their limitations regarding power efficiency and cost.

Analog -Nellcore

One highly analog approach[24] developed by Nellcore aims to filter and amplify the signal to its highest potential before it is sampled by the microcontroller. To this, noise filtering, R/IR separation, DC/AC separation, and AC amplifying are completed in the analog realm in order to use the ADC to its resolution potential when sampling the AC component.
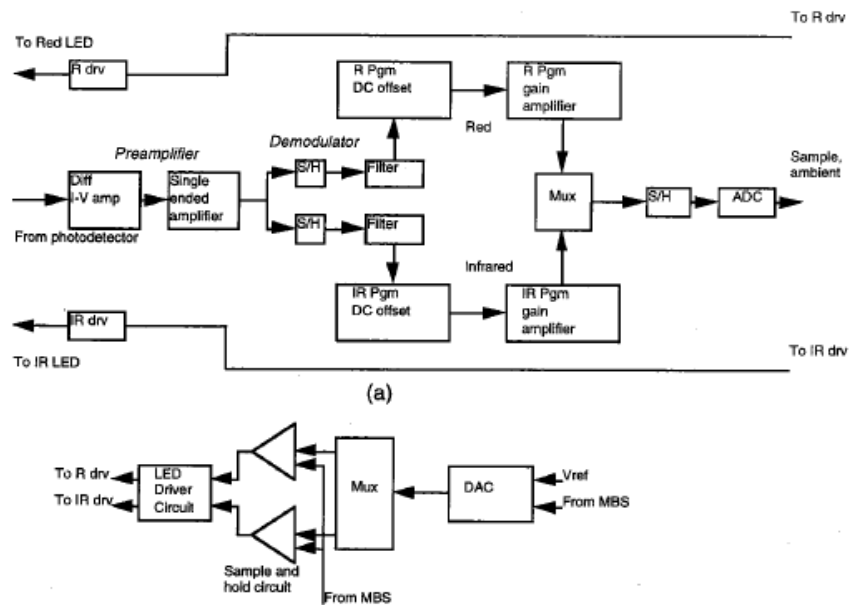
Figure 16: Analog processing system (Nellcore®)

When the photodiode detects light, a current is created proportional to the intensity of the light detected. This current is converted into voltage using a differential current-to-voltage amplifier. This amplification also amplifies external interference, but the differential amplifier produces a positive and negative signal, which can be passed through a single single-ended amplifier. This allows magnitude of the signal to be doubled while much of the interference is canceled out.

Since both the red and infrared LEDs are detected by the same photodiode, and have been filtered and amplified as a single signal up to this point, a sample-and-hold circuit is used for each wavelength. These circuits operated in a manner as to activate when its corresponding LED is ready to be read from the single amplified signal. From this, two signals, a red and an infrared, have been extracted to be filtered and amplified individually. To remove noise, each signal is filtered by a switched capacitor filter so each signal will have the same gain and phase. A second filter in series is then used to remove noise created by the switching capacitor.

Each of these signals now consists of a large DC component and a small AC component which typically only comprises of about 1% of the entire signal. In order to take advantage of the ADC resolution, the DC component must be removed and the remaining AC component amplified. The AC signal consists of the volt range between the highest point of the signal and the lowest point of the signal. The DC component consists of the volt range between the lowest point and zero. An offset amplifier removes this DC component then a programmable gain amplifier amplifies the remaining AC component for the ADC. After this AC component is considered by the microcontroller, the DC component is re-added.

A multiplexer, followed by sample-and-hold circuitry, is used to select either the filtered red or infrared signal to be considered by the ADC. This multiplexer is controlled by the microcontroller and allows the requirement of only a single ADC to handle both the red and infrared signals individually.

LED performance and behavior is an important consideration in pulse oximetry. Since manufactured LEDs are only tested as batches and can tend to be inconsistent in intensity, some form of adjustment to address this must be included in these methods. In this approach, positive and negative thresholds (Figure 19) are created on the ADC, which, when exceeded, cause a size change of the DC component that is subtracted on the programmable gain amplifier. This ensures the ADC is never overdriven.
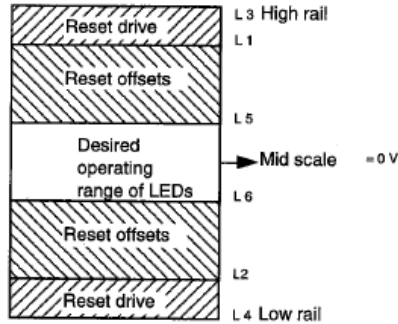
Figure 17: Threshold Range on ADC

In the Nellcore topology, the DAC used to keep the A/D in the desired operating range could be replaced by an automatic gain control circuit. It is therefore possible to get rid of the DAC in this topology. More explanation of this is in the Automatic Gain Control section.

Analog Duty Cycle Limiting Factors

In order to obtain the lowest possible duty cycle, and therefore lowering power consumption, the duty cycle of the LEDs needs to be as small as possible. With a heavily analog topology, the two biggest limiting factors include rise and fall times for the LEDs and photo-detector. Op-amp gain bandwidth and slew rate is also of concern when dealing with fast rise times, but using a topology similar to the Nellcore topology makes this less of a factor. The fast rise time in this topology only affects gain circuitry before the sample-and-hold demultiplexer. After this, the bandwidth of the system drops to below 60Hz. Given that our integrated photo-detector and op-amp light detector has rise and fall times of less than 20uS, unity-gain bandwidth of an op-amp needs to be at least 50kHz. If only a buffering op-amp is necessary with this bandwidth, it is not a difficult requirement.

Digital – Analog Devices

Much of the filtering, amplification, and signal separation completed in the analog realm can be completed in the digital realm as well.

The Analog Devices method[27] still includes the basic current-to-voltage signal conversion using an op-amp, as explained previously, but also introduces other functionality. Included is a current sink controlled by a DAC of the microcontroller to manage the current of each LED and a programmable-gain amplifier and offset, also controlled by a DAC of the microcontroller, to

condition the signal before it is sampled by the ADC. These two implementations work cooperatively, as controlled by the microcontroller, to take advantage of the resolution of the ADC.
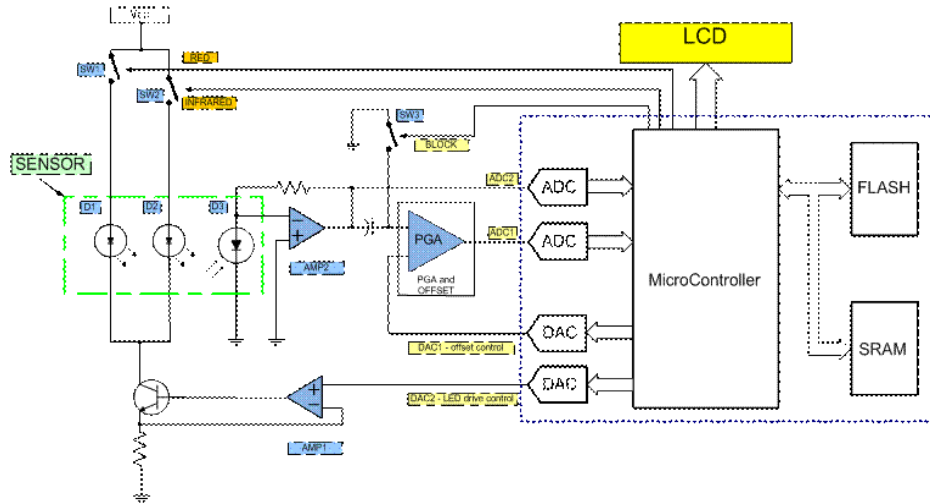
Figure 18: Digital Implementation

The microcontroller tracks the DC voltages from the two LED signals. These DC voltages can then be subtracted from the AC and amplified using a DAC and an op-amp. This topology has the advantage of having almost all of the circuitry on one chip.

Digital Duty Cycle Limiting Factors

As with the analog topology, the LED and photo-detector rise times are limiting factors. The AC amplifying op-amp in the digital topology has strict requirements though. Due to its significant gain and short rise and fall times, gain-bandwidth and slew rate requirements are much greater than a heavily analog topology. Since the AC signal is ~1% of the DC, the gain for the AC amplifying stage needs to be 30-100. Given our 20uS rise and fall time from our sensor, a gain-bandwidth of Gain/(1/20uS) = 1.5-5MHz is necessary. This requires a more expensive and possible power hungry op-amp, or lowering the duty cycle.

Comparison of Analog and Digital

The analog approach uses op-amp circuits for the majority of the signal processing, and the microcontroller as a means of timing and final SPO2 calculation. The signal processing power consumption in this topology can be attributed mainly to the op-amp circuits. With

current op-amps running in the micro-amps, power consumption due to signal processing is minimal.

The digital approach relies heavily on the microcontroller. In addition to all filtering, the microcontroller is responsible for control and adjustment of most of the analog aspects, which will require higher processing power. Since a high capability processor will be required and the lack of downtime available, the device will consume more power.

A simplified comparison can now be made with estimates of cost and battery given the two topologies, using the most expensive and power dissipating parts in the topologies. The Quad Op-amp is an OPA4348 micro-power chip from TI. The Dual Op-amp is a higher performance TLV2373 chip from TI. The DAC is a TLV5616, micro-power chip from TI. The microcontroller is a PIC24F series. These parts were chosen as being inexpensive and low power components.

Table 2: Sensor Topology Cost Comparison

Analog Cost			
Part	Qty	Cost/unit	Cost*unit
Quad Op-amp	2	0.66	1.32
Dual Op-amp (V-I)	1	0.74	0.74
uController w/ ADC	1	2	2
		Total:	4.06

Digital Cost			
Part	Qty	Cost/unit	Cost*unit
Dual Op-amp	1	0.74	0.74
DAC	1	3.5	3.5
uController w/ ADC	1	2	2
		Total:	6.24

Even though the analog topology has 10 op-amps total, it is still less expensive than the cost of one DAC. Eight op-amps will be used for signal processing, and the other two will be used to drive the LEDs. The two op-amps in the digital topology are used for amplifying the AC signals. All costs are prices per 1000 qty.

Assuming that the LEDs are running at the same duty cycle, and the complexity of the microcontroller program is the same, an estimate of the power consumption can be made.

Table 3: Sensor Topology Power Consumption Comparison

Analog Power Consuming Parts			
Part	Qty	mW/unit	mW*unit
Quad Op-amp	2	0.592	1.184
Dual Op-amp (V-I)	1	0.0726	0.0726
uController w/ ADC	1	17.82	17.82
		Total:	19.0766

Digital Power Consuming Parts			
Part	Qty	Cost/unit	Cost*unit
Dual Op-amp	1	0.0726	0.0726
DAC	1	2.31	2.31
uController w/ ADC	1	17.82	17.82
		Total:	20.2026

The power consumption of the digital is topology is roughly the same. It is correct, however, to say that the microcontroller program would in fact run at a higher power. Also, the TLV2373 cannot supply a full-scale output with the given gain-bandwidth. The LED duty cycle would therefore have to increase, or a more expensive op-amp would be chosen. Power consumption would therefore be better with the analog topology. An accurate margin of the power efficiency gains were not estimated, as the cost was also cheaper. It is clear that in this case, an analog design would be better.

This decision also helps in the design stages, as it can be tested almost completely independent of the rest of the system. This will ease in design and prototyping.

2.3 PROJECT SPECIFICATIONS

After evaluating the existing products in the field of wireless pulse oximetry, a series of design requirements were created. The overall requirements of the product were for the design to have a very long battery life, when compared to existing models, and a low unit cost. Specific requirements inherent to the primary goals of the project are described below.

Oxygen Saturation Range: 0%-100%

The device worn by the patient must be capable of measuring SpO_2 values over the entire range, from 0% to 100%.

Oxygen Saturation Accuracy: 70-100% +/-2 %

In order for the product to be clinically useful, the accuracy of the oxygen saturation must be within an acceptable range for values above 70%. At any concentration below this value a patient's health would be in such severe danger as a very precise SpO_2 would be meaningless.

Pulse Rate Range: 30-300 BPM

This range covers most physiologically possible pulse rates. This is an acceptable range for most uses; patients exhibiting behavior outside this range are in the extremes of health. For practical purposes, this range is much more than adequate.

Battery Type: Two 1.5V AA batteries

The battery type selected for this project is a typical, widely available battery of the appropriate size and power density needed for this design.

Operation Time: Min. 100 hours with new batteries

An operational time requirement of 100 hours is comparable to some products on the market, and exceeds that of many others.

Wireless Range: 10m radius

A typical application of this device would be monitoring patients in a medium- to large-sized room. A minimum wireless range of 10m would provide sufficient coverage for most applications.

Operating Frequency: 2.4 GHz center frequency

The 2.4GHz ISM band is particularly useful for this project, as this band is free for use by any device without a licensing fee.

3 PRODUCT DESIGN

The following figures show the high-level system block diagram of the design. The system topology pulls in the signal from the finger sensor, is processed by analog and digital signal processing, and the patient vitals are sent over the air via a wireless link, and displayed through USB to a host computer.
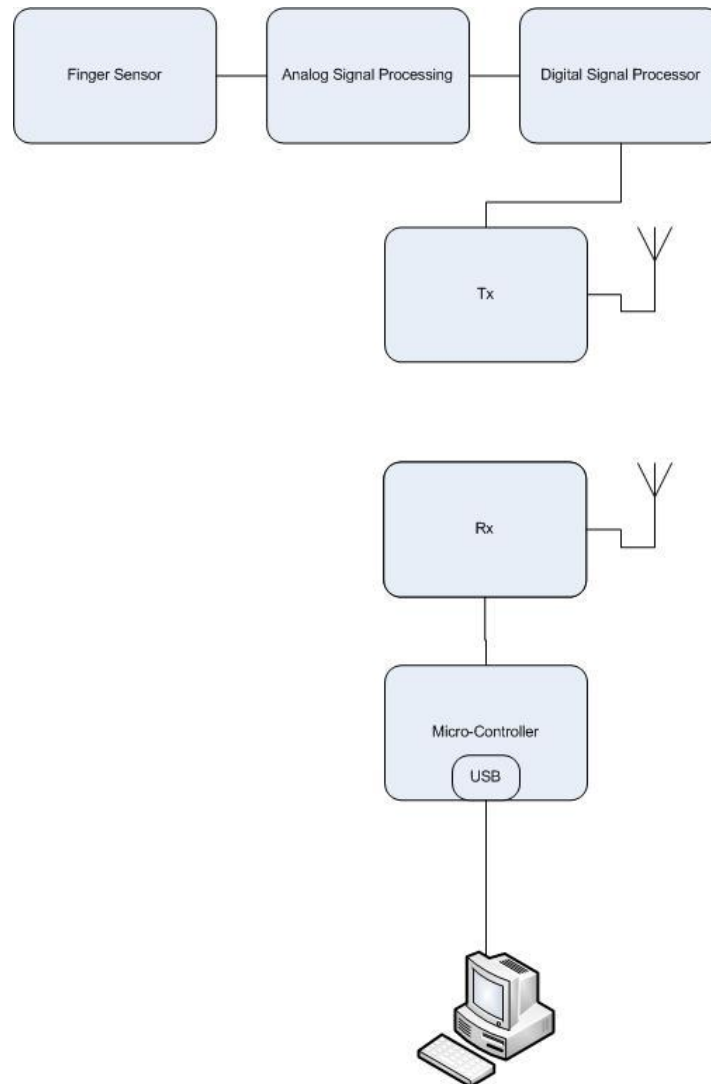

Figure 19: Overall System Block Diagram

3.1 DESIGN OF FINGER SENSOR AND ANALOG PROCESSING

The finger sensor consists of three components, a red LED, an infrared LED, and a light detector. The signal from the light detector is conditioned by the analog processing, which consists mostly of op-amp circuits.
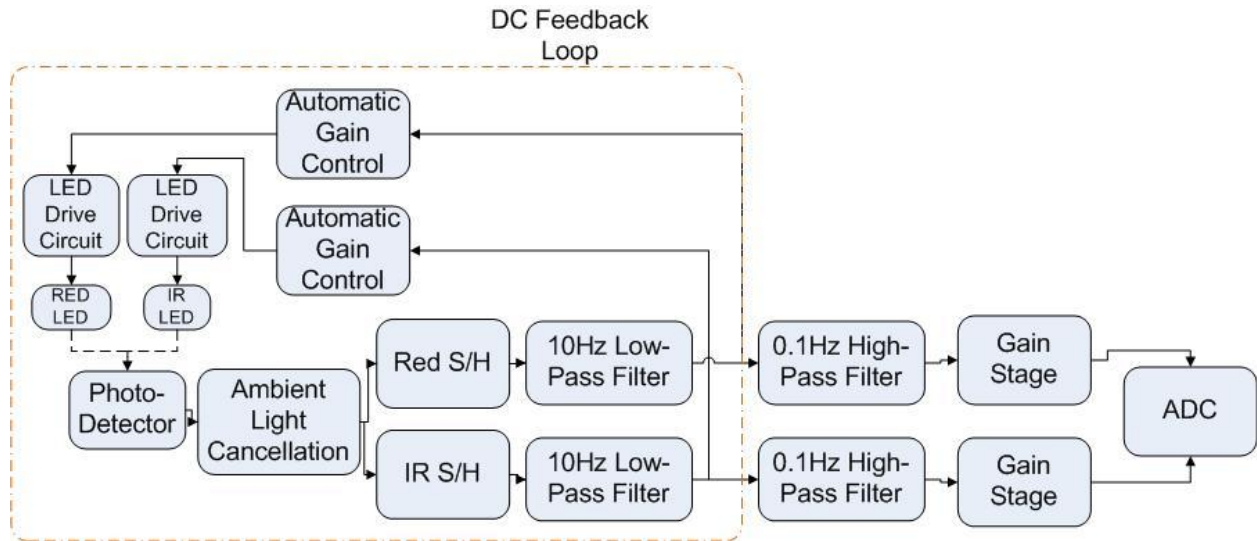
Figure 20: Analog Processing Block Diagram

A completely analog topology was used for the signal processing of the sensor. The multiplexed signal received by the photo-detector is de-multiplexed by two sample and hold circuits. An ambient light cancelling circuit subtracts the amount of light present when both LEDs are off. The outputs of the de-multiplexing are low pass filtered to remove noise introduced through the sample and hold, and the remaining noise from ambient light. At this point, automatic gain controls create a feedback loop, adjusting the brightness of the LEDs so that a constant DC signal is present at the low-pass filter. The low passed signals then enter high pass filtering to remove the DC components. The remaining cardiac AC signals can then be amplified before being sampled by the ADC. Since the automatic gain controls keep the received DC levels the same, only the AC amplitudes are necessary for computation of SPO2.

See the Appendix A for a complete schematic.

3.1.1 Finger Sensor Part Selection
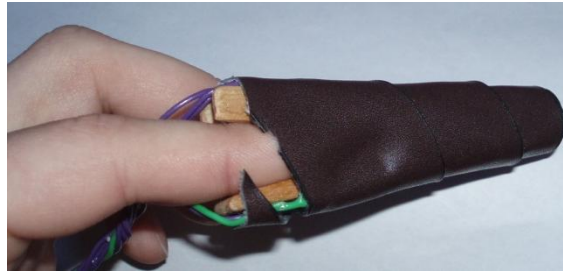
Figure 21: Finger Sensor Prototype

Red LED

The red LED, in particular, has strict requirements. Due to its position on the light extinction curve, unpredictability in the LED wavelength can alter the accuracy of the final SPO2 calculation. For this reason, having a narrow bandwidth, or spectral line half-width, is necessary. Having a wavelength of 660nm is important, because the most research has been done with this wavelength, as it is easy to work with. The deviation from the 660nm wavelength can be accounted for with a wavelength coding resistor. For the sake of simplifying the project, this was not implemented. The maximum pulsed current is crucial, as it is necessary to pulse the LED brightly in order to obtain a quality signal. The angle of the light beam is also a consideration, as a wide angle can waste energy. Any light not received by the light detector is wasted light. Size and mounting ability is also an issue. Too large of an LED would not easily fit in a compact sensor. For these reasons, the LTL-4266N red LED was chosen.

IR LED

The IR LED has looser requirements. Due to its position on the light extinction curve, wavelength accuracy is not a prime concern. Like the red LED, maximum current, beam angle, and size are key criteria. The LTE-4206 was chosen for these reasons.

Photo-detector

The light sensor has to be responsive to both wavelengths of light. One of the most important parameters of interest is the rise and fall time. The faster the times, the lower the duty cycle can be for pulsing the LEDs. In this design, and integrated photo-detector and op-amp pair

were chosen for simplicity of design, fast rise and fall times, and a wide spectrum response. The TSL-12S was chosen.

3.1.2 Finger Sensor Sampling

Ambient Noise Cancelling
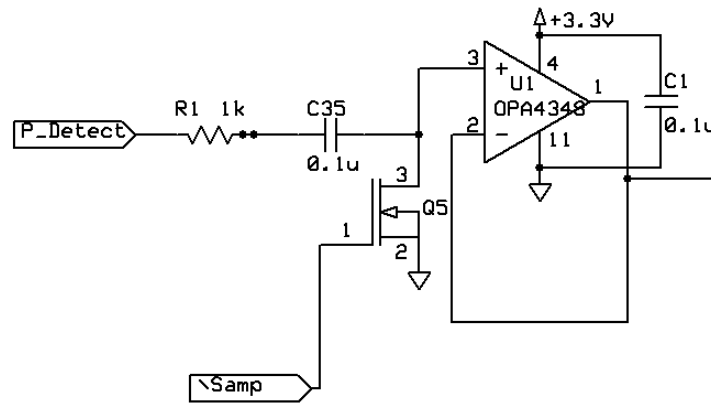
Figure 22: Ambient Noise Cancelling Circuit

Ambient light can introduce significant noise into the system. A switched capacitor light cancelling circuit is an inexpensive solution to removing noise from ambient light[28]. The input stage of the analog processing removes much of this noise by effectively sampling the light level while no LEDs are turned on. This is done by charging a capacitor, C35 when the LEDs are off. The N-Channel MOSFET, Q5 pulls the capacitor to ground to charge it. When an LED is turned on, Q5 turns off, leaving the capacitor in between the output of the photo-detector and the input to the op-amp. The capacitor acts as a voltage drop proportional to the light when no LEDs are turned on. The timing of this can be in Figure 23.
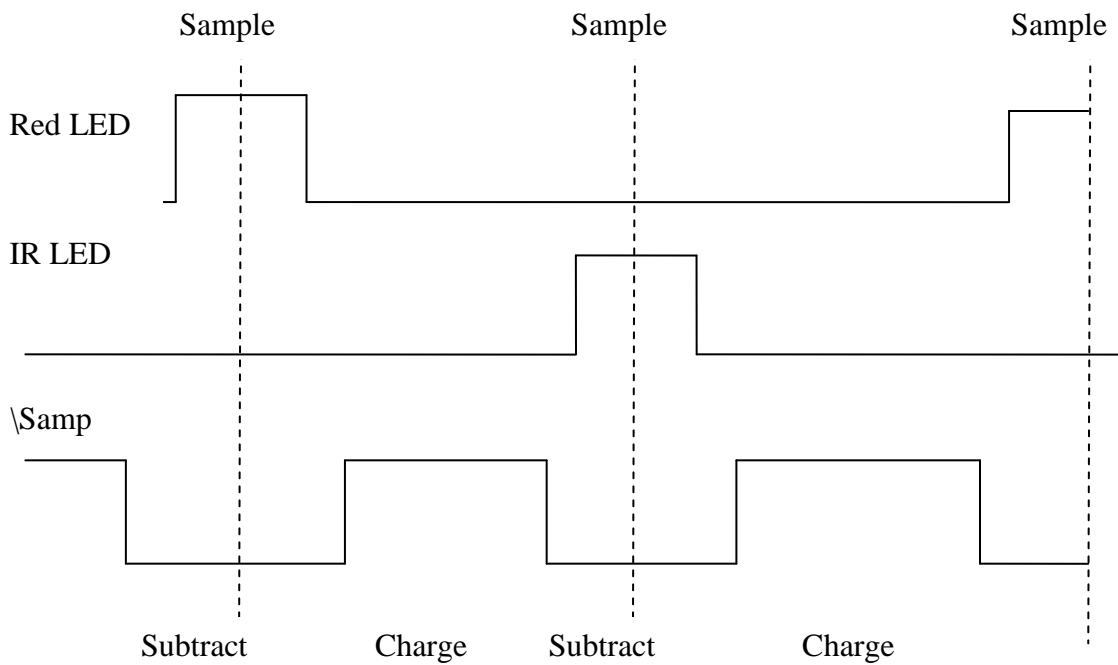
Figure 23: Ambient Noise Cancelling Timing Diagram

As can be seen, when the LEDs are off, \Samp goes high, charging the capacitor. When the LEDs are on, \Samp goes low, subtracting the ambient light.

Sample-and-Hold De-multiplexing
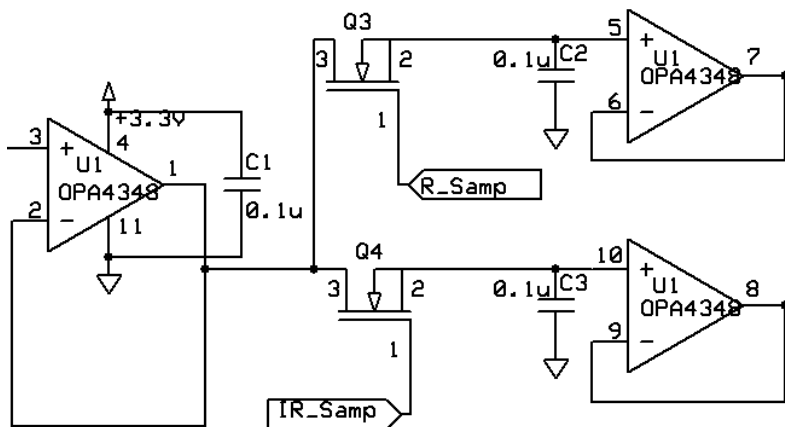
Figure 24: Sample-and-Hold De-multiplexing Circuit

Two sample-and-hold circuits are used to de-multiplex the received signal from the photo-detector into two separate channels. The corresponding MOSFET is driven when the

corresponding LED is turned on. This transforms our pulsed signal into two continuous signals that can be further processed.

A simulation was made using SwitcherCAD, a PSPICE application. The following is the plot of a 30mV signal centered at 3V being inputted into one channel of the sample and hold circuit. The sampling frequency is 150Hz. This is to simulate the type of signal that would come from the photo-detector circuit. Both the input to the sample-and-hold, and output for one channel is shown.
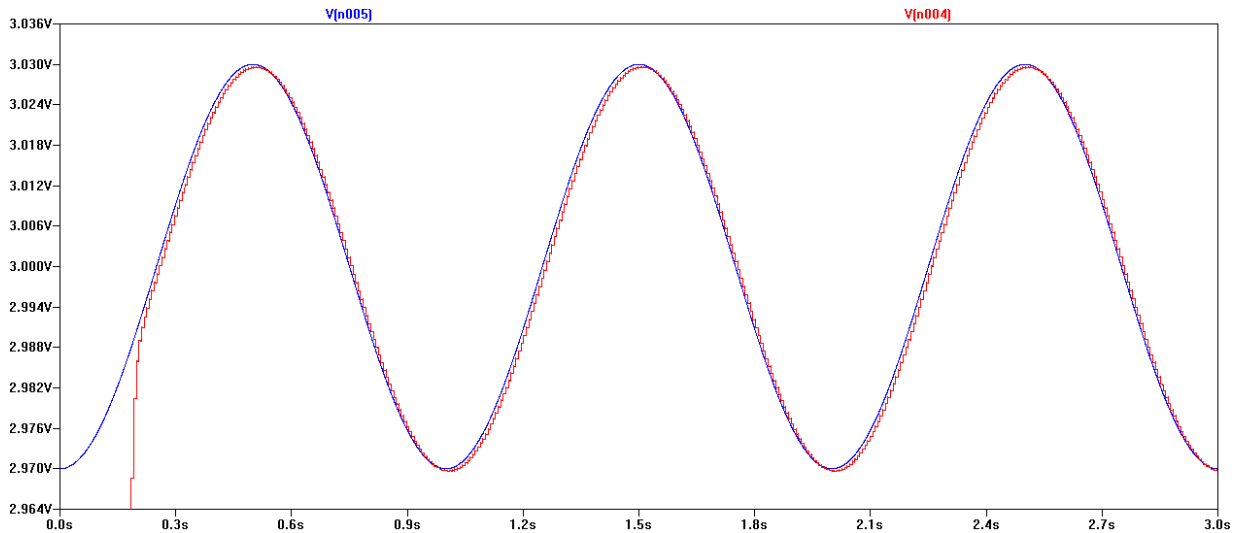
Figure 25: Sample-and-Hold Output

Notice how the outputted signal is close to that of the inputted signal. A cleanly reproduced signal is important to our signal integrity and accuracy.

3.1.3 Signal Conditioning

Passive Filtering
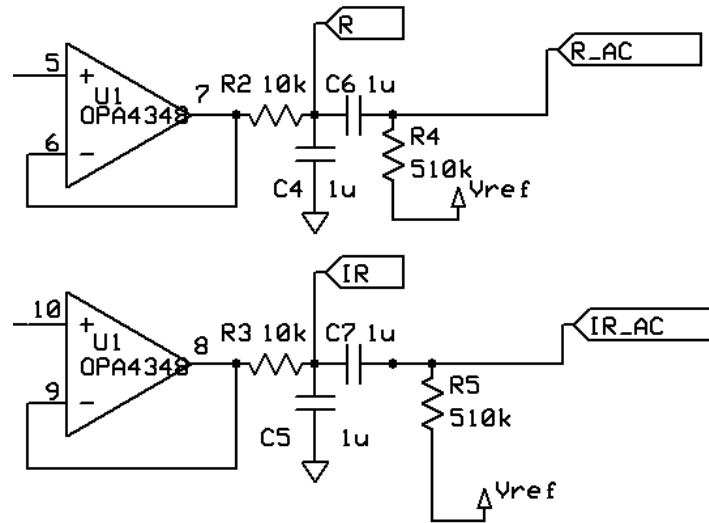
Figure 26: Passive Filtering Circuit

The output of each channel of the de-multiplexer goes through two stages of passive filtering, a low pass filter and a high pass filter (DC blocking). The first stage has a cut-off of about 10Hz. This is used to get rid of the high frequency components introduced in sampling and holding, and to remove 60Hz ambient noise. For our specifications, we want to have a BPM range of 30-300. This corresponds to a bandwidth requirement of at least 0.5Hz-5Hz. A 10Hz filter was chosen so that the fundamental and second harmonic of the cardiac beat could be captured. The high pass filter removes the DC content of the signal and biases it at V_{ref}, which is half of the supply voltage. Figure 27 and Figure 28 plot the gain and phase of the signal after the low pass and after both the low and high pass filters. The solid line represents gain and the dashed line represents phase.
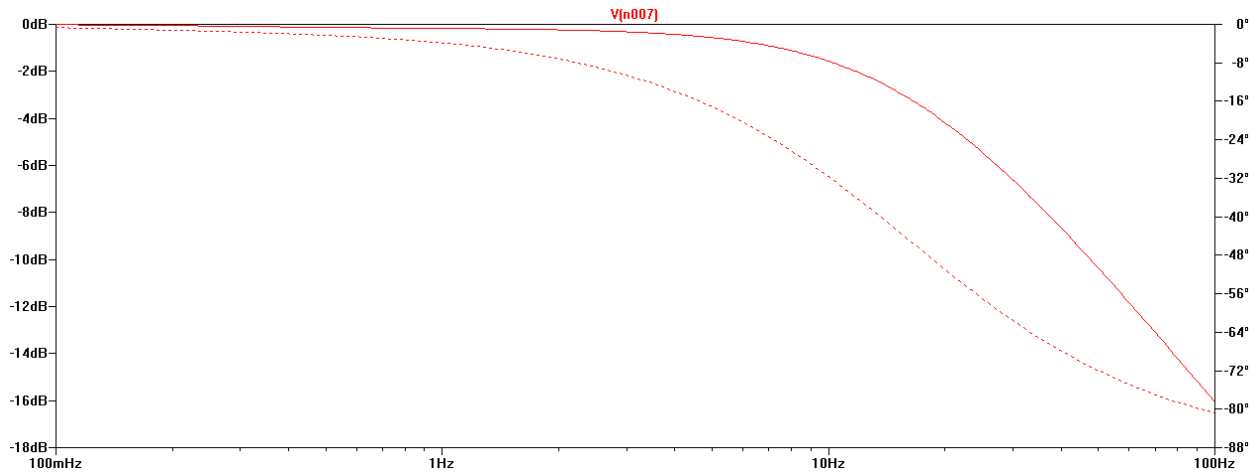
Figure 27: Frequency Response after Low Pass Filter
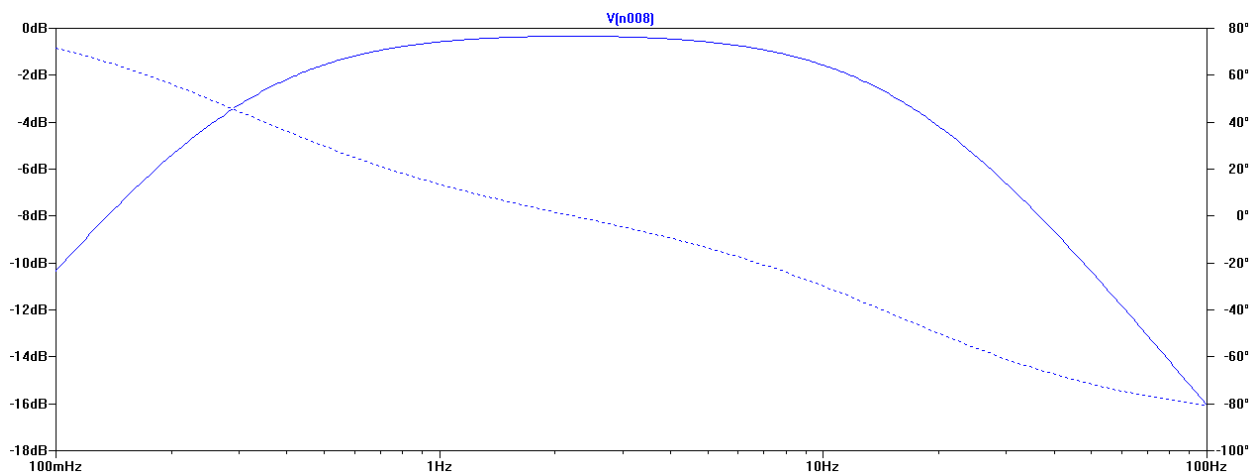
Figure 28: Frequency Response after Low Pass and High Pass Filters

Reference Voltage Source
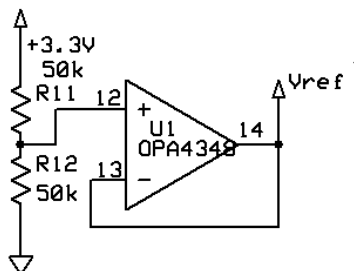
Figure 29: Voltage Reference Circuit

The reference voltage used to bias various signals, V_{ref}, is created using a simple voltage divider and voltage follower circuit. This makes V_{ref} a low impedance source.

AC Gain Stage
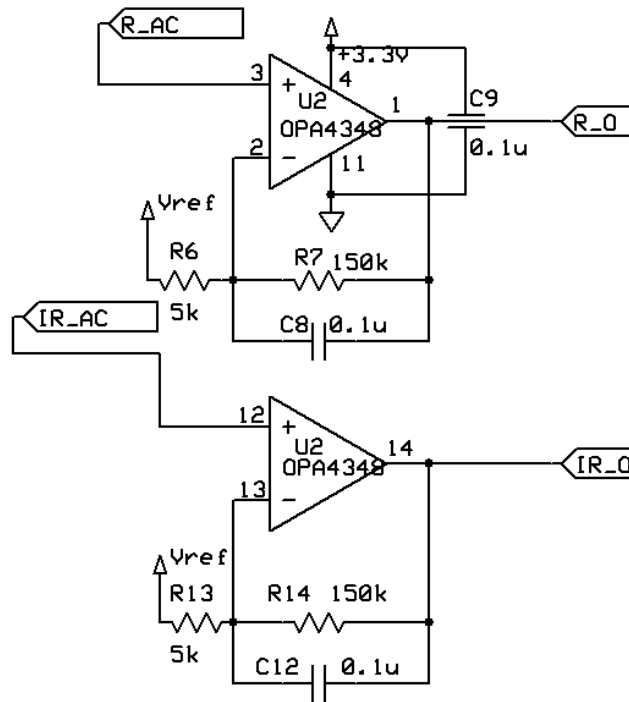
Figure 30: AC Gain Stage Circuit

A single, non-inverting gain stage is used for each signal. This gain is set to 31, and includes an active low pass filter to remove noise above the bandwidth which we are interested in.

The gain for this stage is set to 31for a specific reason. Assuming that the DC content of each channel is 3V, the cardiac component will be about 1-2% of this, or 30-60mV. A gain of 31 will give us a useable AC signal somewhere between 930-1860mV peak-to-peak. This will leave about adequate headroom above and below the signal, which is needed during patient motion to prevent clipping of the signal.

The cutoff frequency is set to 10.6 Hz, similar to the first passive filter. Combining this filter with the passive filtering in the previous stage, a double pole filter is effectively realized. The plot of the gain and phase combining the passive and active filtering can be seen in Figure 31.
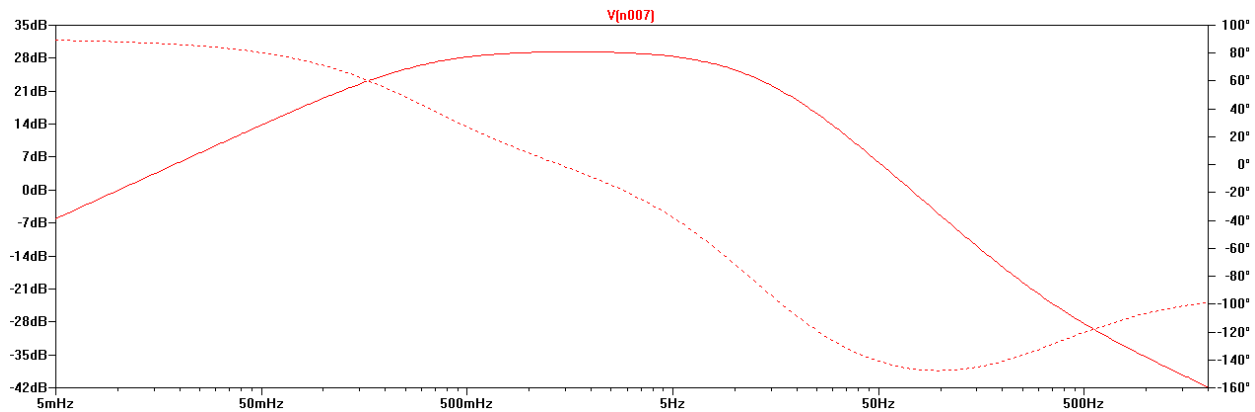
Figure 31: AC Gain Stage, Gain and Phase Plot

3.1.4 LED Driving Circuitry

Voltage-to-Current Converter
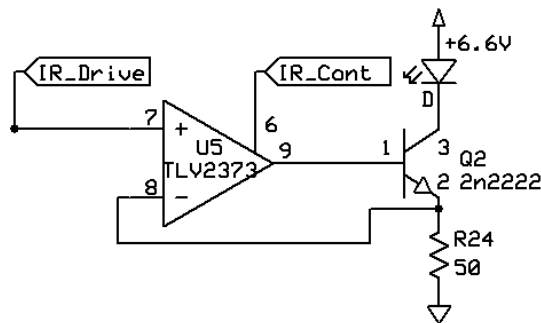
Figure 32: Voltage-to-Current Converter Circuit

An op-amp and npn transistor combination is used to drive each LED. The transistor does the current driving, while the op-amp measures the voltage drop across the emitter resistor (R24 in the diagram). This creates a feedback loop that drives the LED proportional to the voltage applied to the positive input of the op-amp.

An op-amp with better slew rate and gain-bandwidth properties was chosen for better accuracy, as well as having a shutdown pin. This comes at the price of higher power consumption. To counteract this, the op-amp will be shut down when the LED is not being driven. Since the duty cycle for driving the LED will be around 1%, this is significant power savings.

Figure 33 shows the simulated drive current vs. the corresponding input voltage.
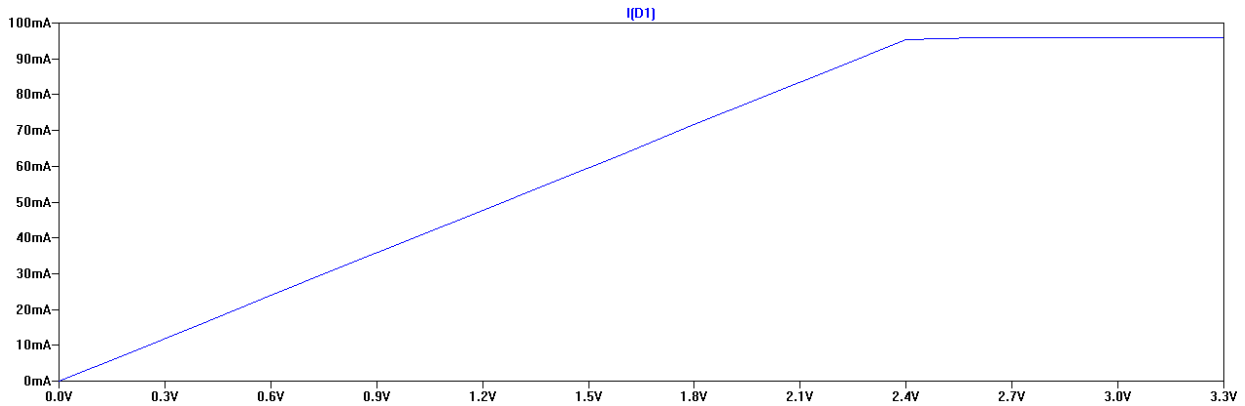
Figure 33: LED Driver V-I Characteristic

The plot is fairly linear until it evens out at about 2.4V. This gives us a good dynamic range.

The LEDs are driven off of the 6.6V supply to provide enough dynamic range in its current vs. voltage characteristic. A lower supply voltage will lower power dissipation at the cost of a narrower range of input voltages.

If the 3.3V supply were used to drive the LEDs, in order to reach enough current, the sense resistor would need to drop down to 2 ohms, and the new plot would look like Figure 34.
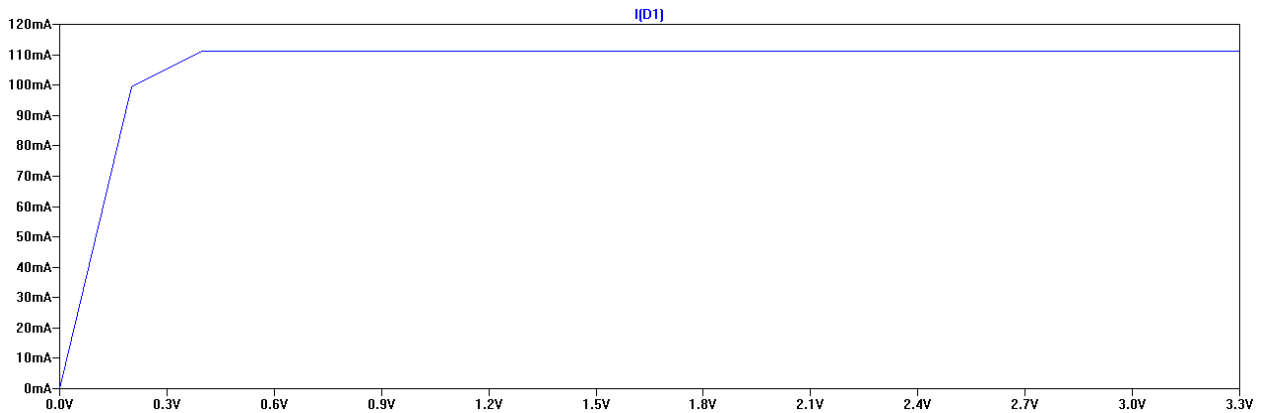
Figure 34: Inadequate V-I Characteristic

In this plot, there is less than 300mV of dynamic range, about ten times worse than the 6.6V supply. This loss in dynamic range would equate to a loss in accuracy of the overall gain control circuitry. As will be explained later, this will lead to a less accurate SPO2 calculation.

6.6V was chosen because it has a good balance between power efficiency and dynamic range. It is also a multiple of 3.3V, which allows the supply to be generated from a high

efficiency charge pump regulator (>90%) off of the 3.3V supply. This circuit is also simpler, and uses cheaper parts, so it is more advantageous to use it in our application.

Automatic Gain Control
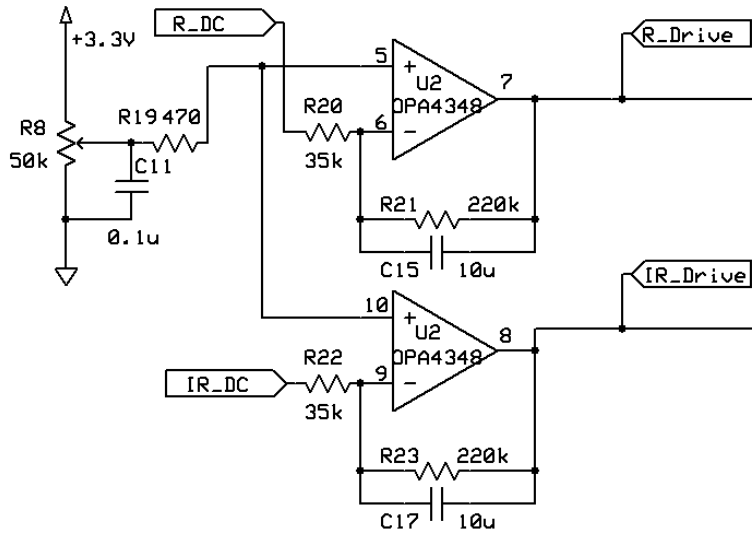
Figure 35: Automatic Gain Control Circuit

Error amplifiers are used to produce the driving voltage for the voltage-to-current converters. They compare the received voltage on each channel to that of a voltage reference set by a simple voltage divider. It adjusts the output voltage accordingly, creating a simple way equalizing the DC voltages of the red and infrared channels. It also serves as a way of changing the light intensity necessary to get a useable signal from different patients. For example, an infant will need less light than a full grown adult. By setting the DC level of the received channels to the same voltage, the DC terms drop out of the SPO2 calculation, allowing us to only need the AC signal being sent to the microcontroller for the calculation.

The effective loop gain of the LED driving feedback loop was simulated using PSPICE. This includes the passive filtering stage after the sample and hold circuit. The solid line in Figure 36 represents gain and the dashed line represents phase.
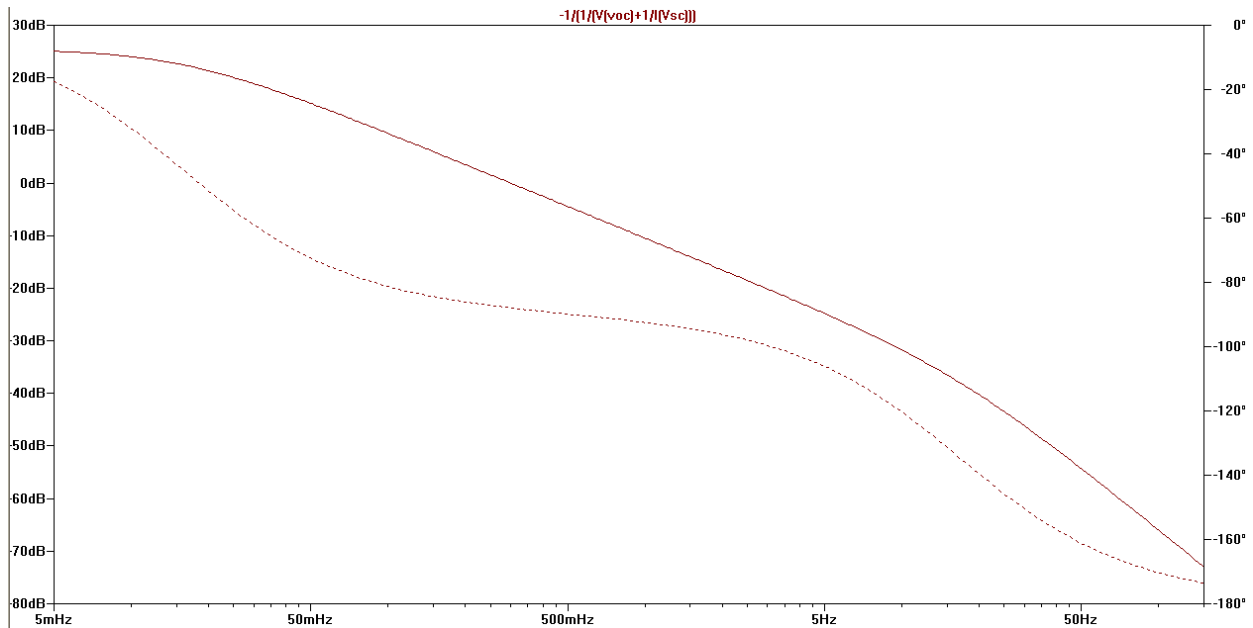
Figure 36: Feedback Loop Gain and Phase Plot

The gain crossover happens at 0.3Hz. This gives leaves a margin so that a cardiac signal of 0.5Hz (worst case) is not compensated for in the feedback loop. If gain crossover were greater that 0.5Hz, cardiac signal would be attenuated. The phase margin is 90°, so it is a good indicator of system stability.

3.2 DESIGN OF DIGITAL SIGNAL PROCESSING

In order to calculate blood oxygen levels, pulse oximeters, in general, use similar methods which include the use of Fast-Fourier Transform (FFT) analysis of red light signals and infrared light signals, and their comparative absorption through a translucent part of a patient's body. For the digital signal processing implementation, this FFT computation is the final result desired, where all previous processes lead to this end result. Procedures leading to the FFT computation include analog system control, analog signal sampling, and signal filtering and decimation. A flow diagram of the final digital system can be seen in Figure 37
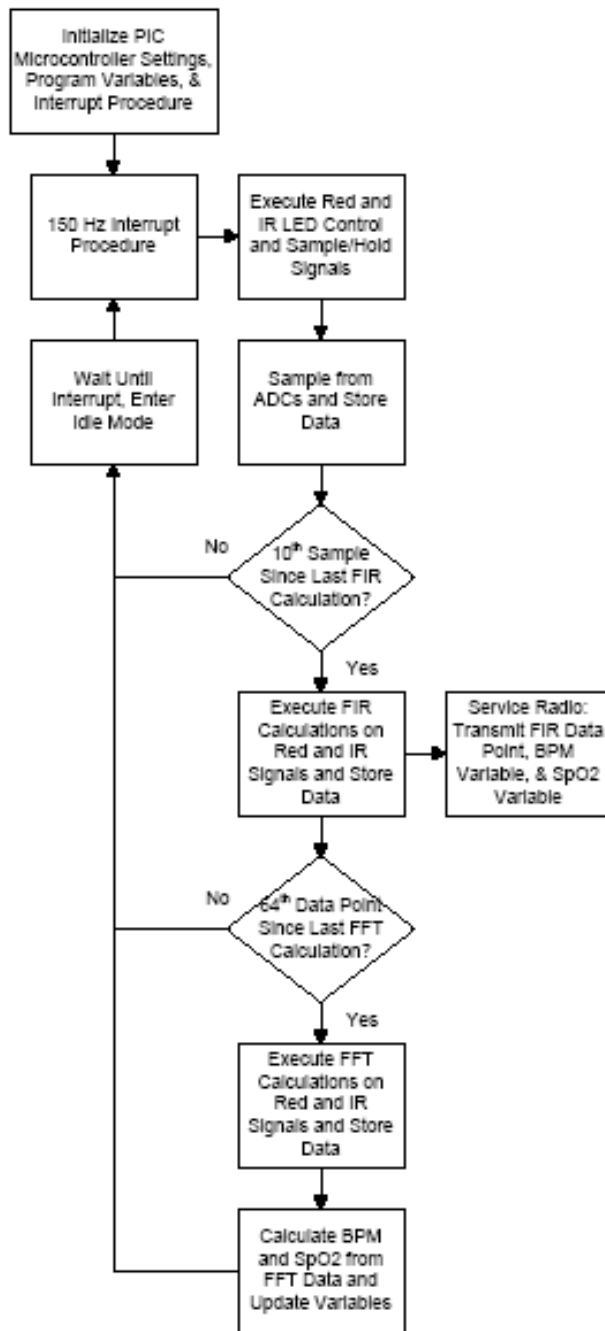
Figure 37: DSP section system flow diagram

This program flow engages the analog circuitry and samples from the red and infrared analog signals. Then it executes a Finite Impulse Response (FIR) filter on both sampled signals to remove noise and other frequencies outside of the cardiac range. Finally, the FFT processes the filtered signals for SpO2 and BPM calculations.

The program and its procedures must follow a certain set of parameters, such as sampling frequency, decimation factors, and filter sizes, to name a few, for proper end results. In order to determine these specifications, the parameters of the desired result (FFT values) must be determined first. The chosen FFT specifications were 64 points with a sampling frequency of 15 Hertz, with an execution time every 4.3 seconds. These parameters were based on the study Optimization of Portable Pulse Oximetry Through Fourier Analysis, by John E. Scharf, MD of the USF Department of Anesthesiology and Terry L. Rusch, BS EE of the USF Department of Electrical Engineering[29]. The purpose of this study was to determine minimum sampling rate and minimum number of discrete data points that retains SpO2 accuracy. This also results in lower power consumption and smaller footprint for portable applications, ideal for this pulse oximeter application and desired resulting behavior. The conclusion of this study is that of the FFT specifications chosen for this implementation.

3.2.1 Timing

With FFT specifications known, the remainder of the program operation parameters can be determined with a balance between power required and accuracy. For our low power application, it was previously determined an acceptable power consumption level would allow a PIC24FJ32GA002 microcontroller to run at 4 MHz for completion of all analog control, DSP, radio servicing processes. An FFT sampling at 15 Hertz, 4 MHz processor, and low duty cycle all become factors for determining program operation.

In order to reduce duty cycle of the microcontroller, analog low-pass filtering was completed before sampling to a cut-off frequency of 7.5 Hertz. This allows the microcontroller to sample from the analog signals at the sampling frequency of 150 Hertz. This sampling frequency was chosen to be able to filter out 60 Hertz noise which is present in most environments. Since this sampling is triggered by an interrupt, efficiency of subsequent procedures becomes a large concern. Many procedures must complete before the next interrupt to prevent program-flow disruption and incorrect data use, however, other lengthier procedures implement the use of buffers in order to execute over multiple interrupt cycles.

3.2.2 FIR Filter/Decimator

The FIR filter and decimator is the middle link between the sampling and FFT processes. The decimator considers the 150 Hertz sampled signal and only keeps every 10th sample creating

the sampling frequency of 15 Hertz for the FFT signal. However, since the sampling rate has changed from 150 Hertz to 15 Hertz, a low-pass filter must be implemented with a cut-off frequency of 7.5 Hertz to compensate. However, only frequencies at and below 5 Hertz are considered.

In order to create the coefficients for this FIR low-pass filter, MATLAB's Filter Design & Analysis Tool was used. Fixed filter parameters included a sampling rate of 150 Hertz and a stop frequency of 7.5 Hertz. Variable filter parameters included the pass frequency, which would affect allowable cardiac frequency range, and pass and stop band attenuations, which would affect filter accuracy. Looser constraints would allow the filter to execute faster with poorer results, and tighter constraints would result in better results with longer execution time. With the timing restrictions previously defined, it was desired to create the best performing filter that was capable of completion between interrupts – within 6.67 milliseconds. The result was an 85th order FIR filter with a pass frequency of 5 Hertz, pass band attenuation of 1 dB, stop band attenuation of 40 dB, and fixed parameters stated previously. The magnitude response of the filter can be seen in Figure 38
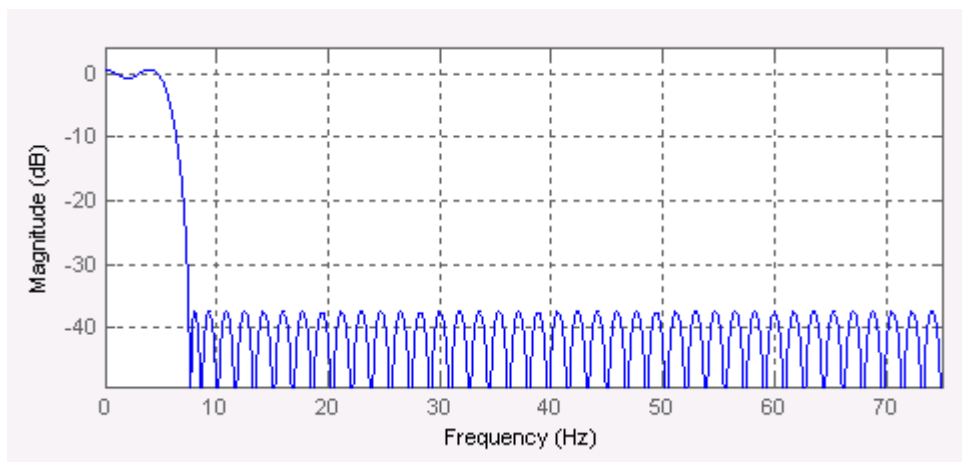
Figure 38: Magnitude Response

The FIR filter and decimator is combined into a single process that is executed after the 150-Hertz interrupt completes sampling. After every interrupt, except for the 10th, each sample is placed into its respective 86-sized array with a rotating pointer, and then waits for the next interrupt. On the tenth interrupt, samples are placed in the array and then followed by FIR execution before waiting for the next interrupt. This code which implements this FIR filter can be seen below.

```
    for (k = 0; k < Nb; k++) {
        FIRred  +=  (long  int)h[k]  *  (long  int)(a1[(oldest  +  k)  %
Nb])/32768;
        FIRir   +=  (long  int)h[k]  *  (long  int)(a2[(oldest  +  k)  %
Nb])/32768;
    }
```

The combination of chosen filter order, fixed-point math (PIC24FJ32GA002 is a fixed-point processor), optimized code, and a rotating buffer allows this filter to finish executing within the allocated 6.67 milliseconds. After execution, the single data point is produced that begins to fill the FFT buffer, with a new value entering the buffer every 66.7 milliseconds – 15 Hertz.

3.2.3 Fast Fourier Transform

The FFT is the final step for being able to determine SpO2 and BPM calculations. As explained previously, this FFT executes every 4.3 seconds. Since an FFT of this magnitude naturally takes a longer time to execute, two 64-sized arrays are used. This allows the FFT to execute on one buffer over multiple interrupt cycles while the filter and decimator process fills the other buffer. Desired low power consumption aside, the only timing constraint on this process would be to finish executing before the next FFT buffer is full – 4.3 seconds, including the time required to service all other processes.

Keeping low power consumption in mind, the execution time of the FFT is reduced by using a number of methods. First, the creation of twiddle factors used in FFT calculation is done once in the initialization stage of the microcontroller. Also, an optimized code implementation is used, although a standard floating-point math procedure is used, a fixed-point implementation could have been used if timing problems arose. Finally, similar to the rotating buffer used by the FIR filter, a lookup table is used when placing values into the FFT buffer in order to perform "automatic" bit swapping. This code which implements this FFT can be seen in Appendix C.

The program counts as one FFT buffer is filled and then calls FFT execution on that buffer once it is determined to be full. A pointer is then changed in order to begin filling and counting the next buffer. Once FFT calculations completes, the result ends in a two 64-sized array, one for each signal. The second half of each array is a mirror image of the first half of the

array, therefore the second 32 values are no longer considered for the remainder of the processes to be executed. With achieving these two sets of 32 values, all data has been obtained that is needed to calculate SpO2 and BPM.

3.2.4 SpO$_2$/BPM Calculation

Data from the magnitudes of the FFT results, at the cardiac frequency, is used in the formula for calculating blood oxygen saturation, which is:

$$SpO2 = -25\frac{AC_{red}/DC_{red}}{AC_{ir}/DC_{ir}} + 110$$

The analog circuitry normalizes the DC values of the red and infrared signals, therefore removing them from this equation. From this, the process for calculating SpO2 only has to consider the peak magnitude from each signal as defined by the first half of their respective FFT results. An algorithm scans these data points and stores the highest magnitude of each. These two values are divided and applied to the rest of the equation, resulting in the patient's blood oxygen saturation percentage.

Beats per minute is determined from considering a zero-crossing algorithm. This is then referenced to FFT data from the infrared signal to ensure accuracy, where inaccurate results are either thrown out or the FFT value is used. The zero crossing is preferable because the resolution of the FFT is approximately 14 BPM. The algorithm counts the number of data points between positive-to-negative zero-crossings over several periods, and takes the average number of data points between these samples. This average sample number is divided by 15, because sampling frequency is 15 Hertz, and multiplied by 60, to achieve "per minute" units. Then largest magnitude from the FFT results is determined, but instead of the magnitude result being stored, the data location (0-31) of the largest magnitude is stored. Due to the Nyquist Rate of the FFT, these data locations would indicate location '0' equaling 0 Hertz and location '31' equaling 7.5 Hertz, with proportionate frequency values in between. This results in a location increment approximately equal to a 0.242 Hertz increment. Therefore, to actually calculate BPM, the data location is multiplied by ~0.242, and then multiplied by 60 to achieve proper "per minute" units. As stated previously, these two BPM values are referenced with one another to ensure accuracy.

3.3 DESIGN OF WIRELESS MODEM

A ZigBee-compliant radio design is shown in the background section of this report to be the preferred approach for creating a robust, secure, and scalable wireless link for this type of S_pO_2 sensor system. However, for the proof-of-concept design being developed for this report, the team decided to use a proprietary 2.4 Ghz RF solution rather than dealing with the licensing and other issues inherent to a full-scale wireless protocol like 802.15.4, ZigBee. One of the chief advantages in using a non-ZigBee system is a reduced protocol stack size, which is very important in reducing the power cost of the system. A smaller-sized modem protocol allows for the use of small, cheap, and power-efficient microcontrollers, which have very limited program memory capacities.   The other overwhelming advantage to a non-ZigBee system is the simplification of the protocol design. A straightforward, "lean" radio interface is ideal for quick implementation, as this project is heavily limited by time. Choosing the correct radio transceiver chip is extremely important in constructing the wireless communication link in this project.

3.3.1 Selecting a Transceiver Chip

In selecting a wireless transceiver module, several points needed to be taken into consideration. The two primary, and equally most important features, are monetary cost and power consumption. As the transmitter and receiver are one of the most power-hungry modules in the design, it is critical that these components consume a minimal amount of energy. Additionally, since one of the goals of this project is to develop a low-cost product, it is very important that the radio solution be as inexpensive as possible. Transceiver chips transmitting on the 2.4GHz license-free ISM bands were selected as the most appropriate for this application, because of a few key advantages:

1. the 2.4GHz band is free for use by unlicensed devices, which is important in reducing the cost of the product
2. there are many low-power choices for 2.4GHz radio components
3. devices operating at 2.4GHz, although shorter range, will have a higher over-the-air baud rate than lower frequency devices, which is useful in lowering the duty cycle and therefore the overall power consumption of this radio modem

In researching these transceiver chips, the following 2.4 GHz devices emerged as the most appropriate for this project:

1. Texas Instrument's CC2500
2. Atmel Corporation's ATR2406
3. Nordic Semiconductor's nrf24L01
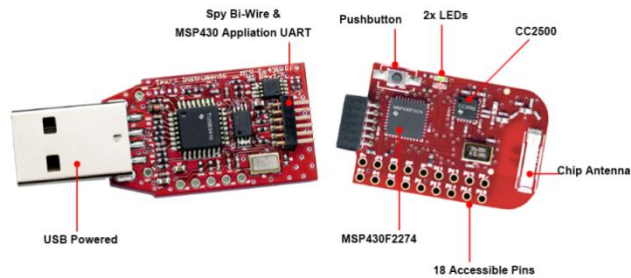
Figure 39: TI CC2500 tranceiver chip, mounted with an MSP430 controller and using a USB interface

TI's CC2500 is a very appealing chip, with many attractive features, such as a high receiver sensitivity of up to -104dB, relatively high output power of +1dBm (maximum), and a low power consumption of 21.5mA in TX mode and 19.6mA in RX mode. The CC2500 also uses a convenient 4-wire SPI interface, and has a minimum number of pins, both considerably simplifying the design process. Still, the CC2500 has some serious drawbacks; primary among its disadvantages is the 240μs power-up delay from the "Sleep" operational mode. In order to limit the power consumption of the radio, this project intends to use the transceiver chip with a very low operational duty cycle. A 240μs power-up delay adds a significant margin to the radio duty cycle, and is a significant disadvantage to the CC2500 chip.

The ATR2406 2.4 GHz transceiver from Atmel Corporation is another radio chip considered for this design. Similar to the TI CC2500, this transceiver is low-power and has good wireless capability, with -93 dBm receiver sensitivity, and a maximum output power of +4 dBm. Power consumption for this chip is 57 mA in active RX mode and 42 mA in TX mode. Although these values are very good, this chip is certainly much more power-hungry
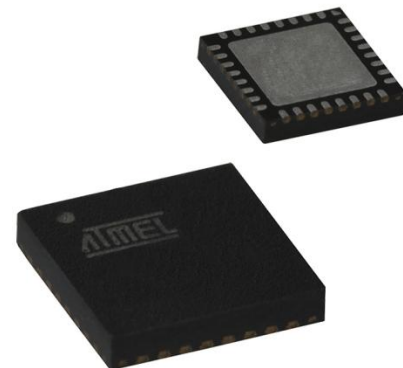
Figure 40: Atmel ATR2406 transceiver chip

than the other two chips that were evaluated for this design. This chip has another disadvantage of a power-on settling time of over 200µs, which, although superior to the CC2500, is still slow enough to inhibit a reduced-duty-cycle design technique.
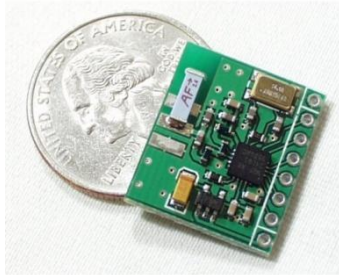
Figure 41: Nordic nrf24L01 transceiver chip; as used in this design, mounted on a breakout board

The transceiver chip finally selected for this design is the Nordic Semiconductor nrf24L01. This transceiver is very similar to the two described above, but outshines both with regards to current consumption and power-on settling time. The nrf24L01 is a low-power 2.4 GHz transceiver, that is intended for devices similar to the one being developed in this project. It has very high RX sensitivity, although not quite as good as the TI CC2500. On the receiver side, the nrf24L01 has -85 dBm of sensitivity, and has a TX output power of 0 dBm. The chief advantage of this chipset is its extraordinarily low power consumption. In RX mode, at 1Mbps data rate (very sufficient for this project), the nrf24L01 draws 11.8 mA of current. In TX mode, the nrf24L01 draws a mere 11.3 mA of power. Although the RF power of this transceiver is considerably less than the TI CC2500, it requires almost one-half the power, which makes it ideal for this project, where extending battery life is a primary concern.

3.3.2 Design of the Radio Protocol

The first step in constructing a radio protocol to fulfill the needs of our system was to develop a list of the requirements for the radio link. The signal processing section of our design needs to output, at the very minimum, the values for the pulse rate and SpO_2 measurements. In addition to this, data points comprising a plot of the sample information from the fingertip sensor can be useful for clinical diagnosis, and also provide a visual display of the proper functioning of the device. The following calculations were performed to determine the number of data bits that needed to be carried through the radio link on each report.

Pulse rate, 30-300 bpm: $log_2(300) = 9$ *bits = 2 bytes*

SpO_2 measurement, 0-100%: $log_2(101) = 7$ *bits = 1 byte*

Signal data point, unsigned integer: *16 bits = 2 bytes*

A total of 5 bytes needs to be transmitted over the wireless radio. The nrf24L01 can transmit data packets with a maximum payload length of 32 bytes, so each data report can be sent via a single packet. Besides determining this data load capacity, the other requirements of the radio connection can be derived from the overall product specifications, and are as follows:

3.3.2.1 Radio Requirements

1. <u>10m Range</u>

To estimate the radio specifications necessary to achieve a 10m range, it is necessary need to determine the free-space path loss at 2.4GHz over a 10m range:

$$FSPL(dB) = 20\log_{10}(d)+20\log_{10}(f)+32.44$$
$$FSPL(dB) = 20\log_{10}(\textit{10m/1000m per km})+20\log_{10}(\textit{2400MHz})+32.44 = \underline{60.04 \text{ dB loss}}.^{**30}$$

This means that the difference between receiver sensitivity and transmitter output power needs to be at least about 60 dB, although this is a great simplification. The nrf24L01 chips used in this project satisfy this requirement, so long as a duck antenna is used (in this case, with 2dBi of gain and a length of about 10cm[31]).

2. <u>2.4GHz Operating Frequency</u>

The operating frequency of the radio system is 2.4GHz-2.525GHz, as dictated by the radio transceiver chip. This keeps the system within the ISM bands, which are free to use by unlicensed devices.

3. <u>Star-type Network Configuration</u>

To simplify design, the network configuration of the radio protocol will be a "star" type configuration, with remote sensors reporting back to a base stations. There are more complicated network topologies that could extend the range of the sensors, but they are far more difficult to implement and were deemed impractical for this project.

[**] Note: this equation for link-loss is a serious simplification, and does not account for a number of factors including multipath fading and antenna gains

3.3.2.2 Radio System Diagram

After determining the necessary functions of the radio communication link, the next step was to develop a radio protocol that fulfilled the requirements. Several features of the nrf24L01 can be taken advantage of here. The chip has built-in auto-acknowledgement of a successful packet transmit, built-in auto retransmit, and Cyclic Redundancy Check (CRC) error detection. The radio protocol developed in this project will take advantage of all of these features. Below are the two system block diagrams describing the operation of the transmitter and receiver radio protocols.

Transmitter System Block Diagram

Receiver System Block Diagram
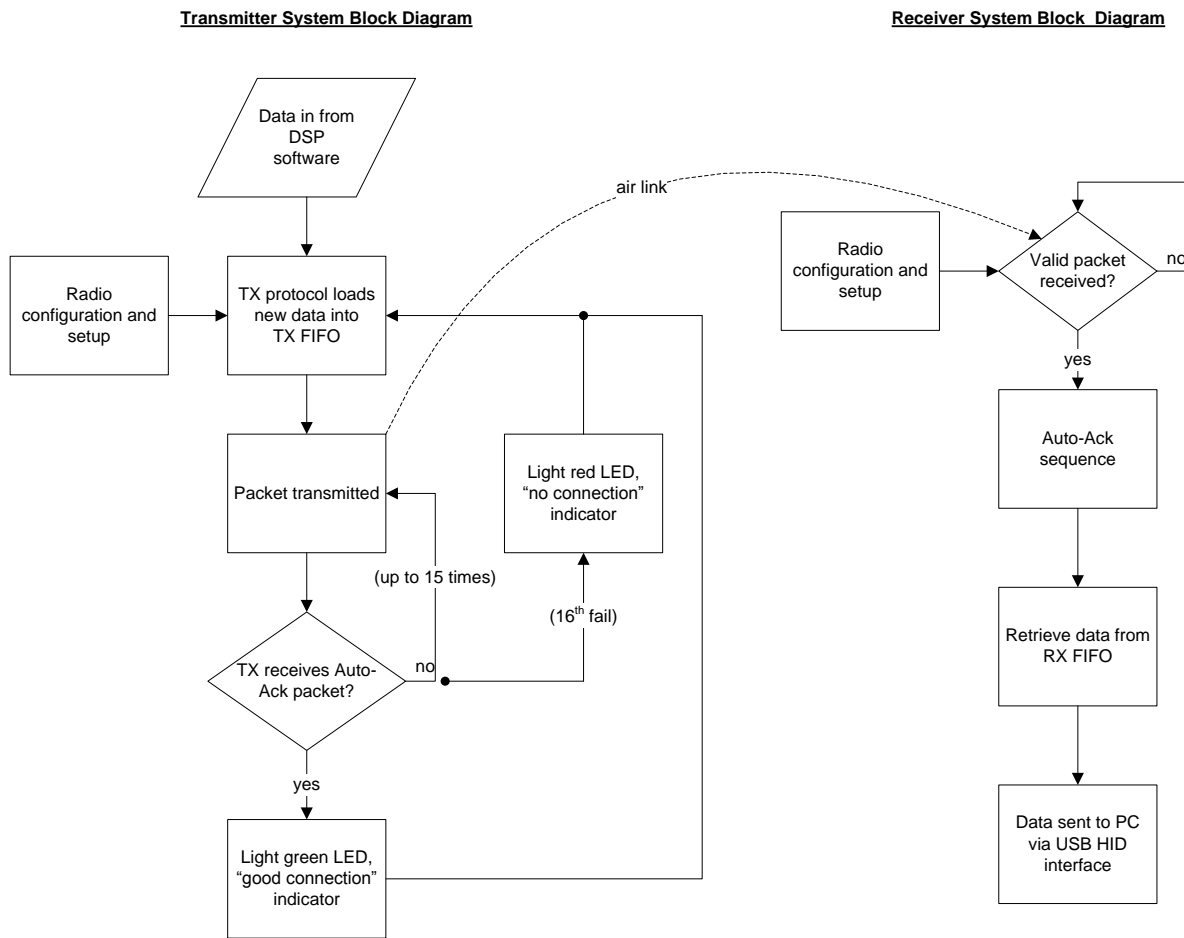
Figure 42: Radio transmitter and receiver system block diagram

3.3.2.3 Transmitter Protocol Operation

The transmitter protocol is in actuality embedded within the DSP code on the remote sensor, on the PIC24F. In developing radio control functions, several important considerations were kept in mind. First, the built-in Auto-Acknowledgement and Automatic-Resend feature of

the nrf24L01 were enabled. Since data reports were to be transmitted at 15Hz, each packet send-receive cycle can take up to 66 ms (operating at 100% duty cycle). This means that the maximum number of automatic resends can be the maximum allowed, or 15, which increases the robustness of the connection (each packet is transmitted up to 16 times total or until a packet gets through). The transmitter system also reports back whether a packet transmission has been successful or unsuccessful, by lighting either a green or a red LED, respectively.

The radio functions quite simply. Commands are sent from the MCU to the radio via Serial Peripheral Interface (SPI). The radio needs to have its setup registers configured on every power on reset. Data payloads are clocked into the TX FIFO on the nrf24L01 chip, and then the radio is brought from the low-power Standby-I Mode into the TX Active Mode to transmit the packet. The nrf24L01 then handles the auto-acknowledge and auto-resend procedures autonomously, once the appropriate setup registers are configured properly. If a packet does fail to transmit, after all the auto-resends, the radio drops the packet, lights the red LED, clears the TX FIFO, and prepares to send the next packet of data.

3.3.2.4 Receiver Protocol Operation

The radio receiver protocol functions as depicted in Figure 42. The first step in the receiver protocol is the initialization and setup of the nrf24L01. After the initialization code is completed, the radio goes into the RX Active Mode and waits for a valid packet. If a new, valid packet is received, the radio returns an Auto-Acknowledge packet to the remote sensor, retrieves the data from the RX FIFO. The receiver device is connected to a Windows PC via a USB HID interface. Because the radio receiver is powered from a computer's USB port, the radio can be run at a high duty cycle. The radio will be in the RX Active Mode for nearly 100% of its duty cycle. In order to further mitigate some of the RF-performance drawbacks of the nrf24L01, the base station device uses a higher-sensitivity 10cm duck antenna, which increases the sensitivity of the receiver unit to hopefully ameliorate the usual interference found at the 2.4GHz band.

3.3.3 Radio Design Conclusions

The radio communication link between the remote sensor and the USB base station is an important part of this design. In order to provide a reliable, low power RF connection, the radio needs to both overcome the interference inherent to the 2.4GHz band as well as limit the duty cycle of the radio transmitter. By implementing the Auto-Resend and Auto-Acknowledge

features of the nrf24L01, the reliability of the wireless connection is significantly improved. The radio transmitter operates at a very low duty cycle, emphasizing power conservation. By implementing many of the built-in features of the nrf24L01, power conservation and radio link reliability can both be conserved, and the wireless connection can satisfy the requirements of this project.

3.4 DESIGN OF POWER SUPPLY CIRCUITS

It is necessary to produce two regulated voltage supplies from the two AA batteries. The 3.3V supply powers most of the analog signal processing, the DSP, and the radio. The 6.6V supply is used to power the sensor LEDs and sample and hold circuit.

3.4.1 3.3V Supply
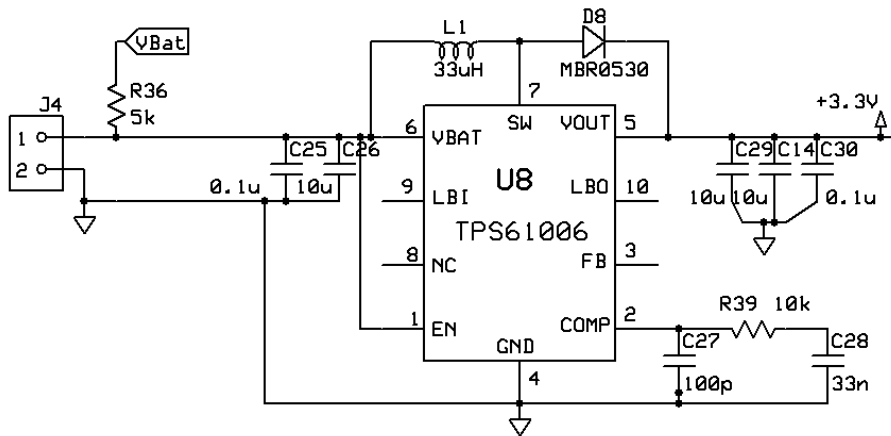
Figure 43: 3.3v Regulator Circuit

A voltage regulator is necessary to take the varying voltage from the two AA batteries (0-3.2V) and power the photo-detector, op-amps, microcontroller, and radio.

The TI step-up regulator was chosen for its low cost, optimization for low current loads, and ease of design. This is a fixed regulator, so no feedback network is necessary, reducing the footprint of the circuit during layout. The 33uH inductor was chosen with a balance between price and efficiency. The shottkey diode, MRB0530, was chosen for its low price and moderately low voltage drop.

3.4.2 6.6V Supply
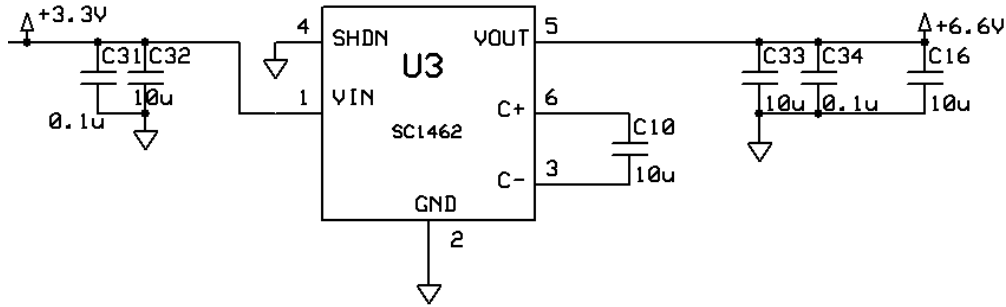
Figure 44: 6.6v Regulator Circuit

A separate 6.6V supply is used to drive the sensor LEDs, and to drive the sample-and-hold MOSFETs. A charge pump voltage doubler is used to double the 3.3V supply voltage. This is done by switching and charging C10.

Since the 6.6V supply is primarily used to drive the sensor LEDs at high currents, noise induced onto both the 6.6V and 3.3V supply is a concern. Using simplified models of the two power supplies, a simulation was made showing the induced noise on each supply in the worst case load scenario.
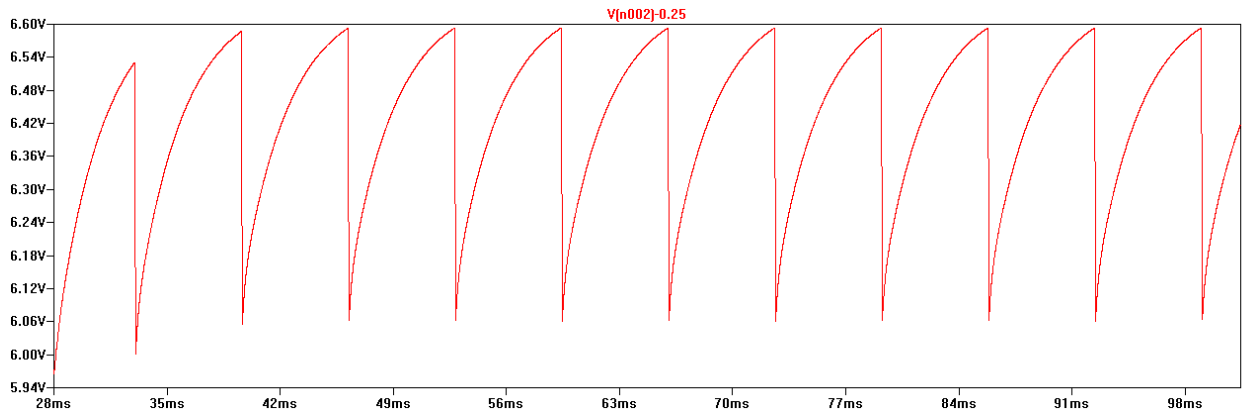
Figure 45: 6.6v Simulated Noise

The induced noise on the 6.6V supply is about 500mV pk-pk. Since this power supply only powers the LEDs and driving circuit for the Sample and Hold, this noise is within a tolerable level. What limits the tolerable noise is the lowest voltage level. The 6V valley leaves enough of a driving voltage for the MOSFETs of the Sample and Hold circuit.

The current draw from the output of the 6.6V regulator shows that the maximum current draw from the regulator is 30mA, and for most of the period, is below 10mA.
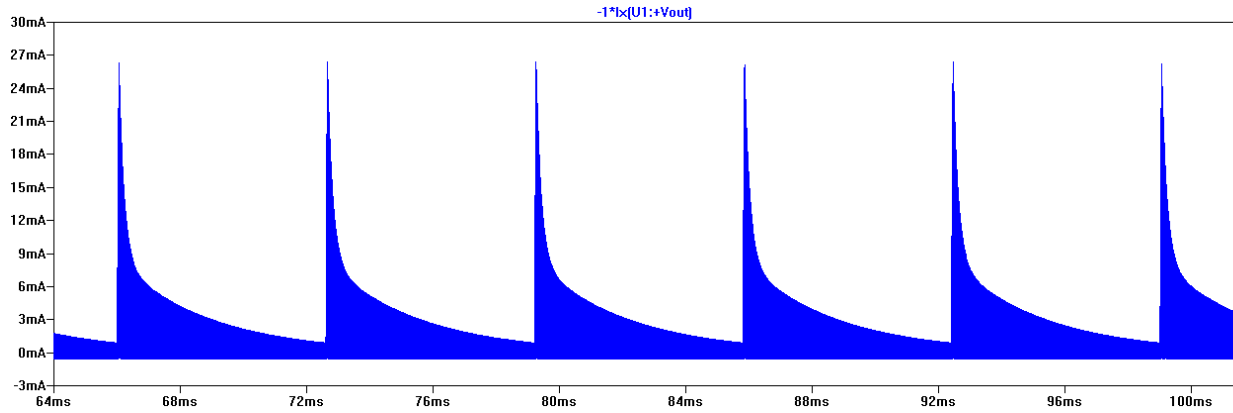
Figure 46: Current Waveform for 6.6v Regulator

The current characteristics are important simulate, as the maximum current on the regulator should not be exceeded. In this case, it is not.

What is of more concern is how the load induces a noise voltage on the 3.3V supply. Using a model of the 3.3V supply as a voltage source with 10 ohm source impedance, the following plot was developed.
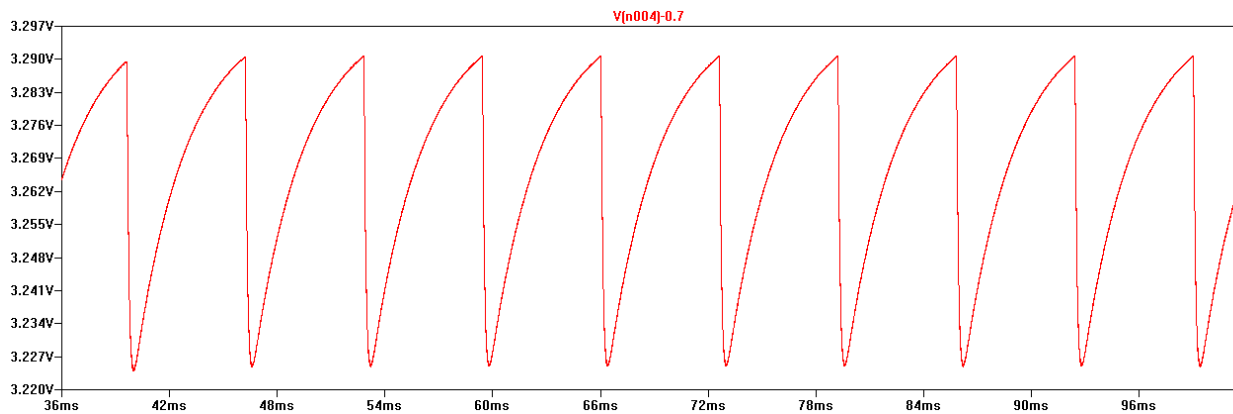
Figure 47: 3.3v Simulated Noise

Because of the large filter caps, the induced noise voltage onto the 3.3V supply is less than 100mV. It is therefore unlikely to produce enough of a noise voltage to cause noise problems in the system.

The current characteristics of the 3.3V supply are also reasonable, with peaks at 8mA.
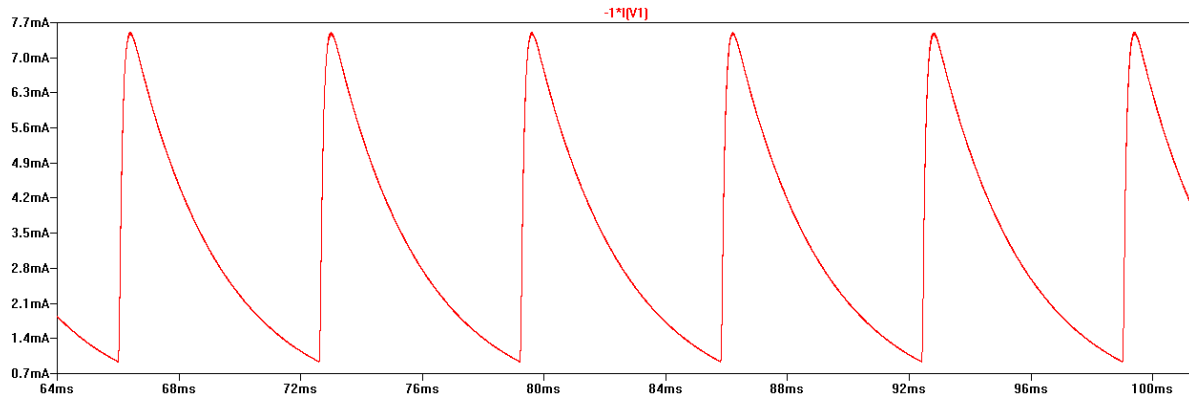
Figure 48: Current Waveform for 3.3v Regulator

The effects of load induced noise appear to be within a manageable level within both the 3.3V and 6.6V supplies.

3.4.3 Battery Life Estimation

Having a battery run low is a risk to the patient. Though not implemented in firmware, the necessary hardware design was accomplished for a battery gauge. An estimation of the amount of time left with the current set of batteries could be continuously calculated based on the battery voltage and current. The battery voltage is measured directly using the microcontroller A/D. The battery current is estimated based on a few parameters. The current draw due to the microcontroller and radio are estimated based on their mode of operation. The current draw due to the LEDs is estimated based on the input voltage to the LED drive circuit (voltage to current converter).

An estimate could then be made as to how much current is being pulled from the battery. A lookup table could then used to predict the amount of time left on the batteries, which is sent to the radio to report.

4 PRODUCT VERIFICATION/VALIDATION

In order to ensure the effectiveness of this design, it was necessary to evaluate each section of the design separately using distinct methods for each respective section. This element-by-element approach is the most efficient way to validate the design, and guarantee that each of the product specifications laid out at the beginning of the design process were met.

4.1 ANALOG SENSOR TESTS

4.1.1 LabView Test Program

Most of the testing of the analog sensor was done with an early, bread-boarded version of the design. Using LabView, a program was written to read the red and infrared signals from the sensor prototype, display them with moderate filtering, perform spectral measurements (FFT), and calculate pulse rate, ratio R, and SPO2.

A block diagram of the system setup can be seen below.
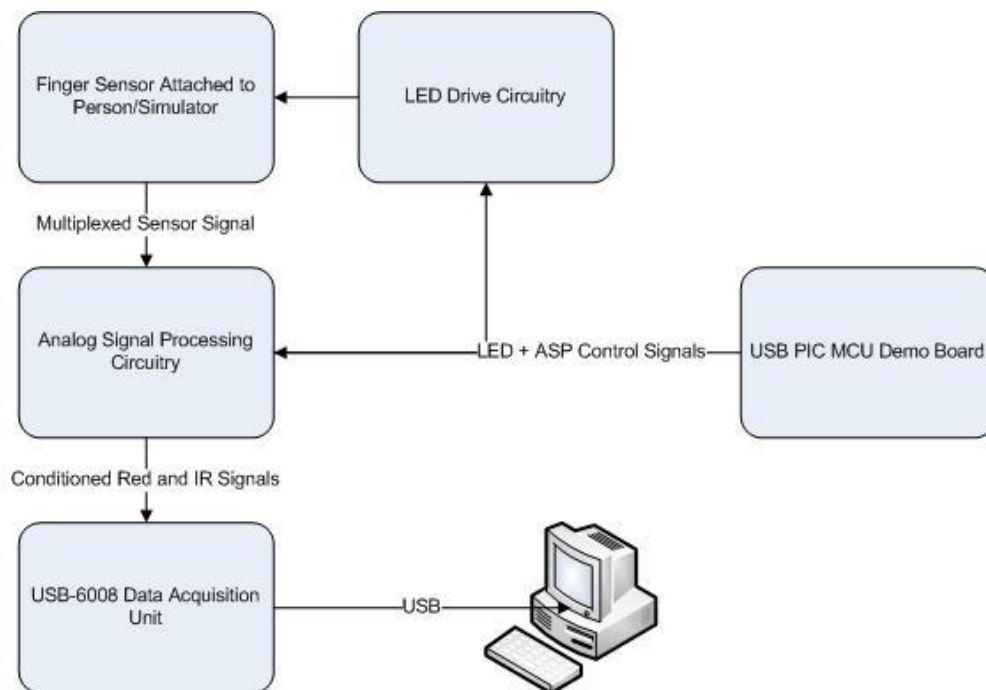
Figure 49: LabView Test Circuit Block Diagram

A PIC microcontroller Demo board was used to create the control signals for the sample and hold circuits and LED driving on the sensor. This was able to be reprogrammed on the PC

in order to allow easy manipulation of the duty cycles for the LEDs. This was instrumental in lowering the output power of the LEDs, while verifying full functionality and signal quality.

A National Instruments data acquisition box (USB-6008) was used to record the measurements. Two 11 bit A/Ds were used. To simulate the effects of using a 10 bit A/D in the final design, the maximum voltage input was set to double the actual voltage. This effectively used only 10 bits.

The completed test system can be seen below with the finger probe attached to a Patient Simulator, and an early version of the sensor.
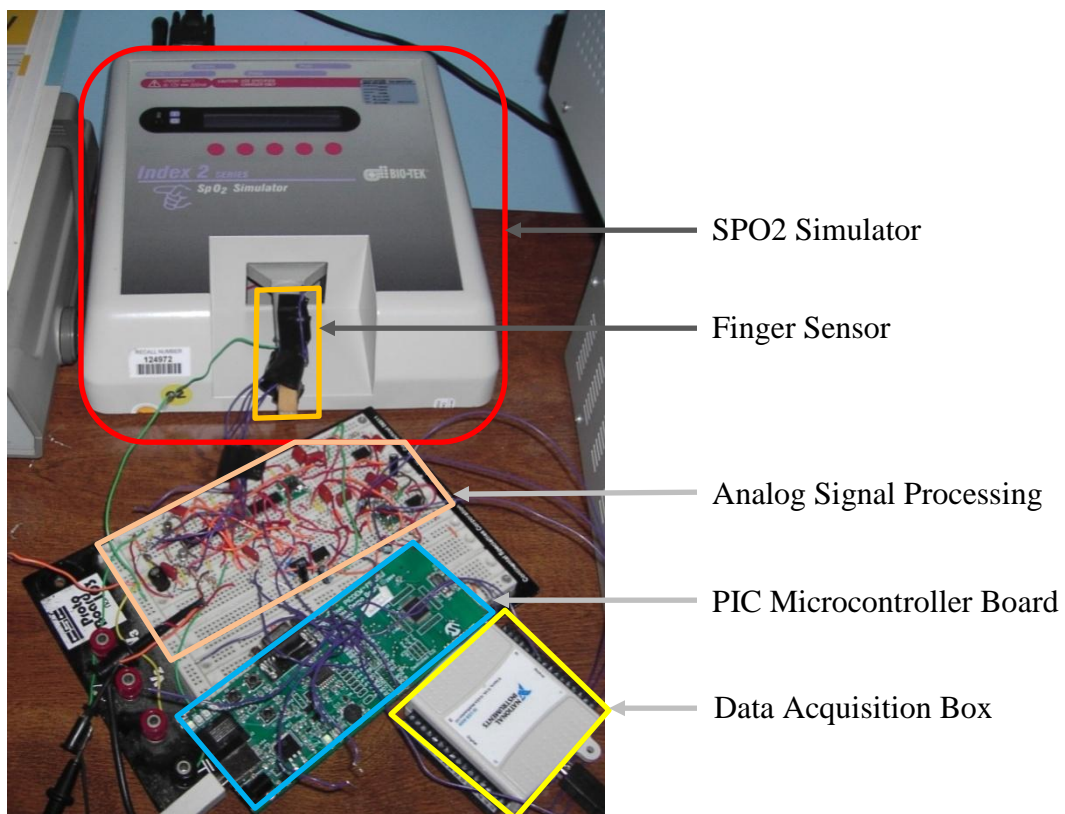
Figure 50: LabView Test Setup

Once the red and infrared LED signals are into the computer, a simple LabView program processes the information. A sample output of this program can be seen below, acquiring a signal from Joseph's finger.
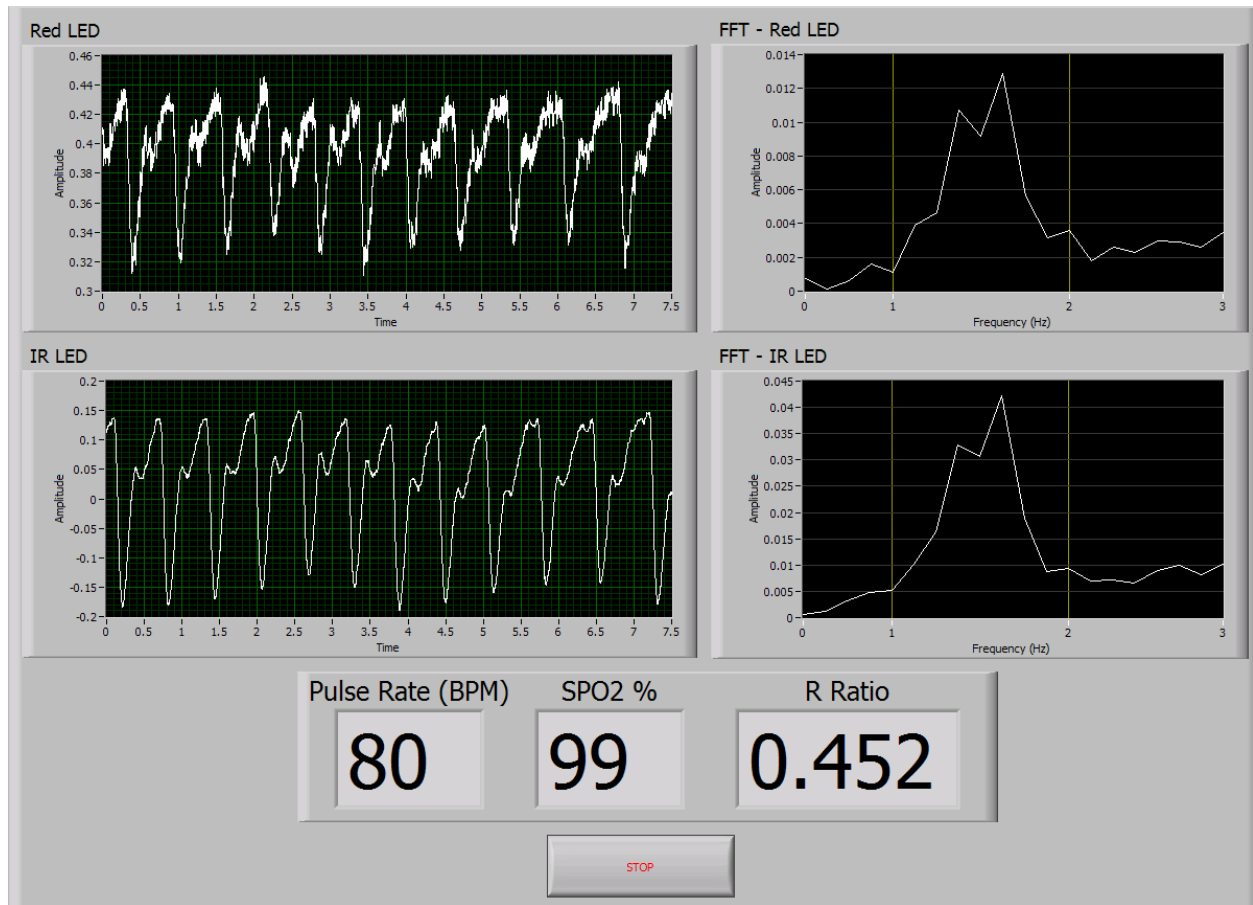
Figure 51: LabView Test Program

The graphs on the left show the digitally filtered signals from the analog sensor. A low pass FIR filter was used with a cutoff frequency of 40Hz. On the right are FFTs of the corresponding channel. The ratio of these two is used to determine the R Ratio, and from there, the SPO2 %.

A simplified block diagram of the test program can be seen below.
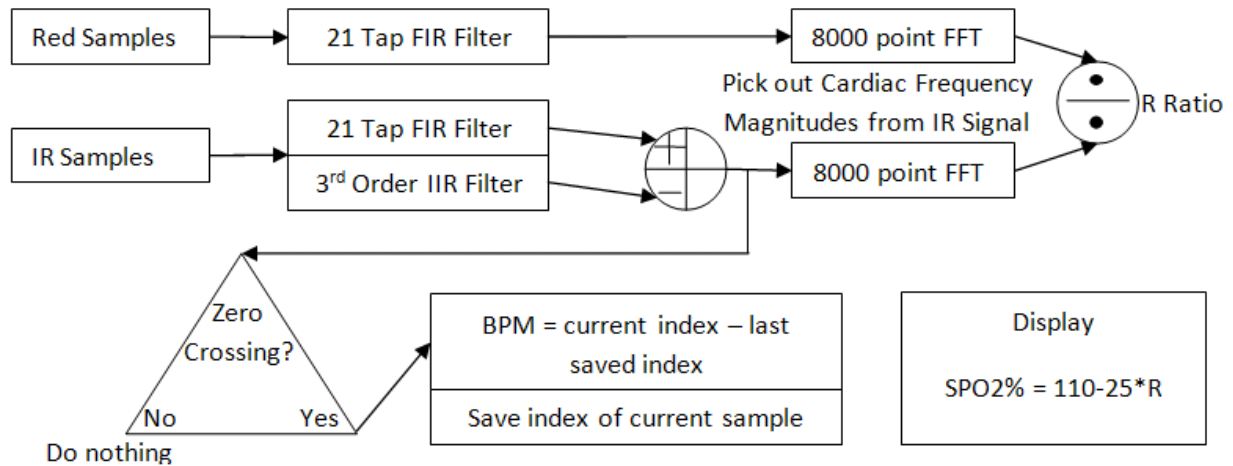
Figure 52: LabView Test Program Block Diagram

The Red and Infrared samples go through simple filtering, to clean up the signal before graphing, running the FFTs, and calculating the BPM through a zero crossing method.

4.1.2 Automatic Gain Control

The accuracy of the SPO2 calculation is highly contingent on having equal DC voltages for the Red and Infrared received signals. The automatic gain control was tested by placing a finger inside of the sensor. Measurements of the DC outputs from the respective sample and hold circuits were then measured. The error of the AGC was then found to be better than 1%. As with the AC gain, this relates to an SPO2 error of less than 0.25%. This test was done seven times for statistical significance.

4.1.3 SPO2 Simulator Testing

Accuracy testing was accomplished using the Index 2 SPO2 simulator from BioTek. There were some initial problems getting the simulator running, as our light source was too dim to be picked up by the unit. This is not a fault of our unit, but a strong point. Due to our sensitive photo-detector and efficient light pulsing, the average power output from the LEDs is very small. Through a combination of increasing the light output and using the simulator's own LEDs, it was possible to test the accuracy of computing the R value. Due to limitations of the simulator, this was only done for a cardiac rate of 75 BPM at saturations of 75% and higher. The test revealed that from 75-100% saturation, accuracy is +/- 2 digits. This is comparable to units

currently in the field. Since this testing was done on an early version of the sensor, further testing in this area would be necessary in order to completely verify functionality.

4.2 DSP TESTS (SIMULATIONS)

4.2.1 Timing

With timing being a large concern for the digital signal processing, testing had to be performed to ensure the execution time of certain aspects of the processing procedures complete in time allotted by the sampling frequency, as determined by the analog portion of the project. This testing was completed by using the stopwatch function of the MPLAB simulator. By setting the simulator frequency to the target 4 MHz operating frequency and placing break points around certain areas in the program, execution time of these processes can be measured.

To begin, execution of the FIR filter must fit within the allotted time. Since the FIR filter executes on a single buffer, filtering must be completed before the next sample. The analog section calls for a sampling frequency of 150 Hertz, therefore, this filter process must complete within the 6.67 ms between samples. Using the stopwatch feature, it was determined on the nine samples from decimation that are thrown away, an execution time of approximately 40 us is required. For the tenth sample kept in decimation, an execution time of approximately 6.4 ms is required, a time just under the allotted 6.67 ms.

The other timing constraint is that of the execution of the FFT. Since the 64-point, 15 Hertz FFT executes every 4.3 seconds, the calculation must also complete under this time. The FFT uses two buffers, therefore, the execution can be calculated over multiple 150 Hertz interrupts while the other buffer fills. Again, using the stopwatch, it was determined the FFT calculation takes approximately 385 ms to complete – a time less than the allotted 4.3 seconds.

To find the duty cycle of the system, all these times are considered over the entire execution of a single FFT. The non-used sample time from the filter can be ignored due to its insignificance size, but the 6.4 ms time is considered. This 6.4 ms calculates one of the 64 points for the FFT, therefore the entire FIR filtering time for a single FFT is 410 ms (6.4 ms * 64). This is then added to the actual FFT execution time of 385 ms to achieve a total time of 795 ms per FFT. Hence, the duty cycle of the system is approximately 20% (795 ms/4.3 seconds), rounded up slightly to compensate for unconsidered execution time.

4.2.2 FIR Filter/Decimator

In order to test the procedures of the signal processor, the MPLAB SIM debugging tool is used to run tests in a simulation environment. Since there are no external signals in the test environment, two arrays are used – one containing the data points for a 1 Hertz sine wave and one containing the data points for an 8 Hertz sine wave. When the interrupt process is triggered, data is pulled from these arrays and filled into the filtering buffers in place of actual data that would have been sampled from the ADCs.

For testing purposes, the 1 Hertz sine wave is used as the red signal and the 8 Hertz sine wave, which should be mostly filtered out, is used as the infrared signal. The results from the simulation of the FIR filter and decimator can be seen in Figure 53.
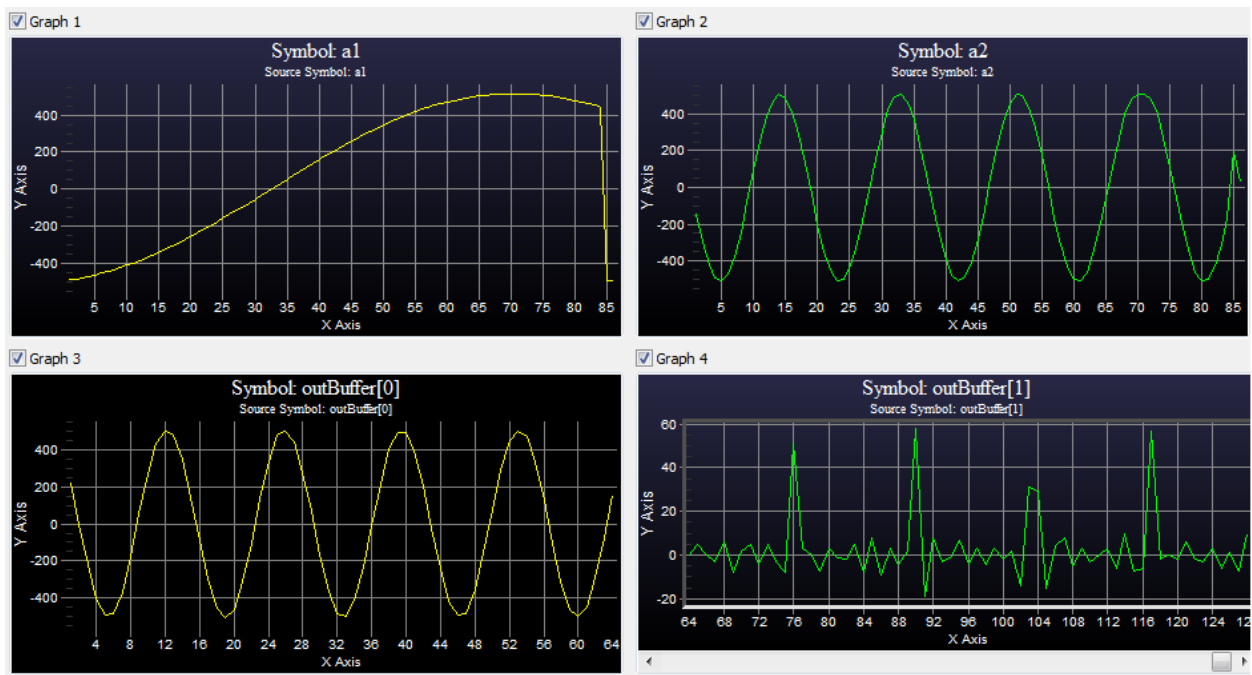
Figure 53: Sample Signals and Filtering

The two left graphs of the figure are from the 1 Hertz signal (red) – on the top is the 1 Hertz signal as it enters the filtering buffer and the bottom is the result of filtering. It can be seen that the signal maintains its full amplitude and is reduced to a 15 Hertz sampling frequency because there are approximately 15 data points per period. The two left graphs of the figure are from the 8 Hertz signal (infrared) – again, on the top is the 8 Hertz signal as it enters the filtering buffer and the bottom is the result of filtering. Since this 8 Hertz is above the 7.5 stop band, the signal is greatly attenuated. Although the signal was not completely diminished, this level of attenuation will not affect the FFT results when compared to the pass band signal.

4.2.3 Fast Fourier Transform

For proper operation of an FFT, data points must be moved around in the array by bit swapping their data locations. As filtering for each data point completes, it is placed in its proper bit swapped location so swapping does not have to be completed later. This data is placed is the real portion of the FFT filter buffer while the imaginary portion of the FFT buffer is filled with zeros. The resulting arrays appear in Figure 54.
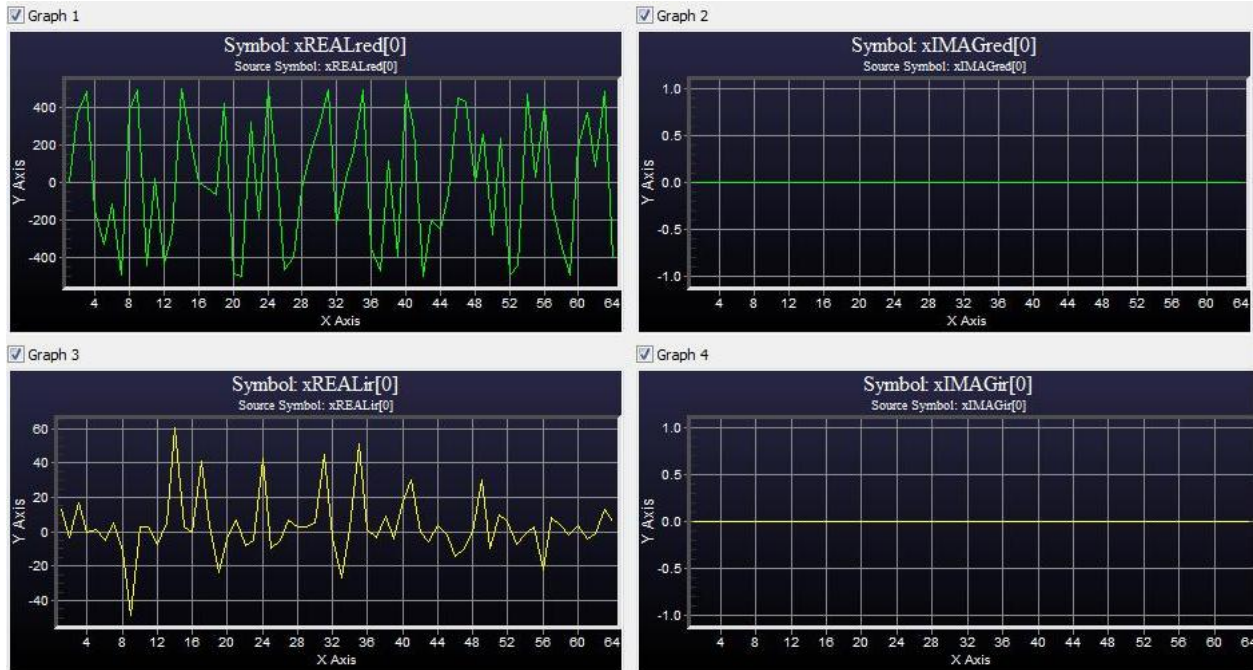
Figure 54: FFT Buffers Pre-Calculation

On the top of the figure, the filtered 1 Hertz signal has been placed into the bit swapped FFT buffer. Although this signal no longer appears as it did originally, the magnitude of the data points have not been changed. On the bottom of the figure, the attenuated 8 Hertz signal has also been placed into its bit swapped FFT buffer. At this point, the FFT algorithm is executed on these buffers and placed back into the same buffer. The result can be seen in Figure 55.
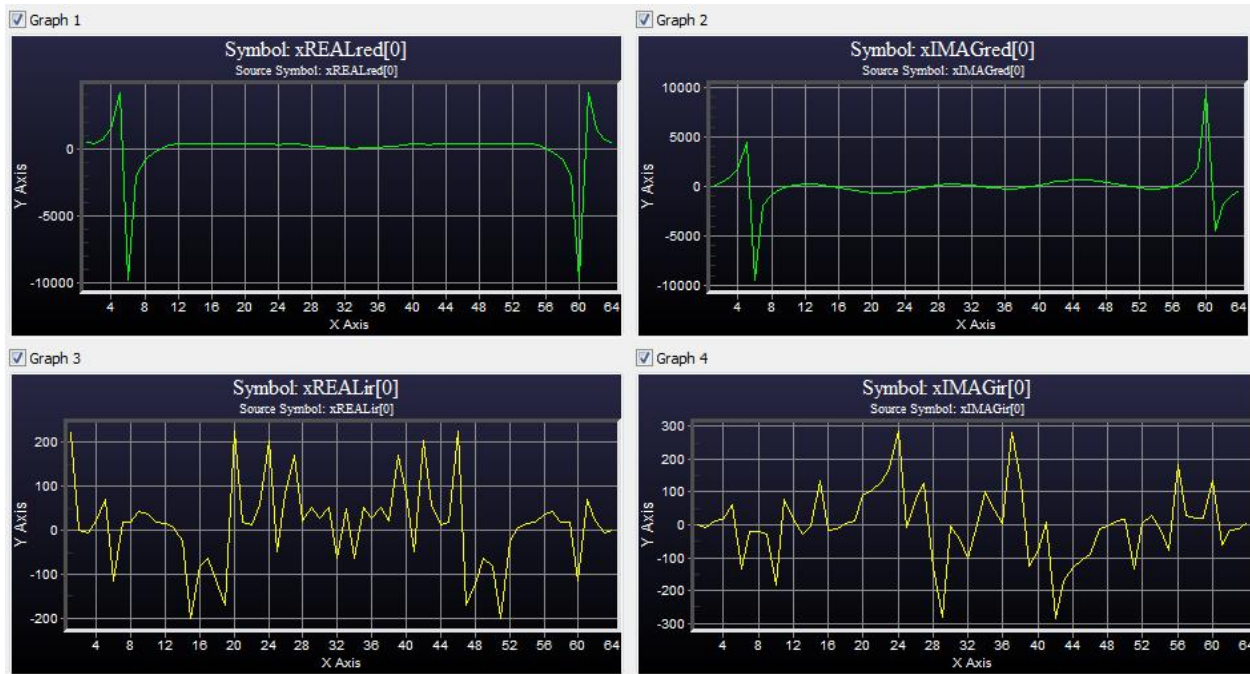
Figure 55: FFT Buffers Post-Calculation

The desired results of the FFT are beginning to show in the 1 Hertz signal (top) with the two mirrored peaks. The attenuation of the 8 Hertz signal (bottom) in the FFT results also begins to show its effectiveness when comparing magnitudes of each of these results. The final calculation to complete the FFT is to take the magnitude between each signal's real and imaginary parts. The result is shown in Figure 56.
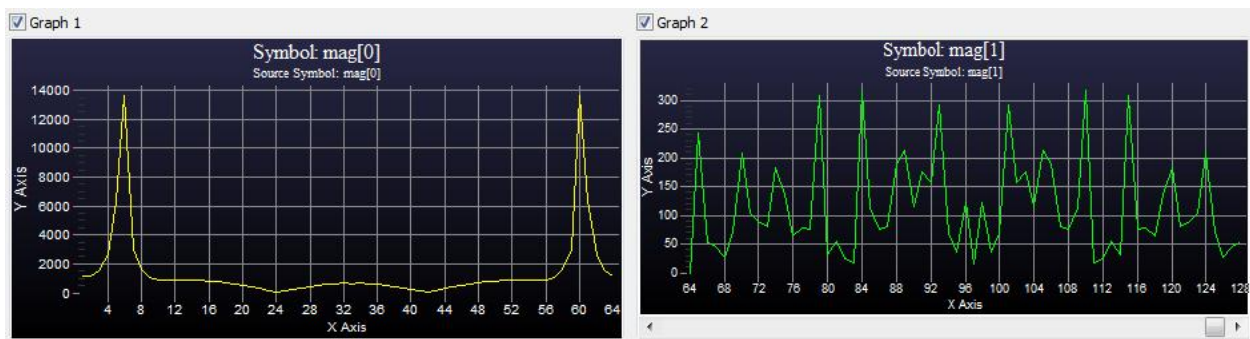
Figure 56: FFT Magnitude Result

The final result of the FFT behaves perfectly for picking peak magnitude values for SpO2 and BPM calculations. Since the magnitude values of the 1 Hertz signal (top) and the attenuated 8 Hertz signal (bottom) differ so greatly, even if this was a mixed signal, the desired frequency can easily be determined with undesired frequencies present.

4.3 RADIO TESTS

After a functional radio protocol was designed, it was necessary to validate the design with regards to the product requirements. The first test was a range test of the radio. A transmitter/receiver pair was tested at several distinct distances, from under a meter distant to up to approximately 15m. The line-of-sight tests were successful up to 15m with no dropped packets. The second test was performed with a single metal-stud sheetrock wall in between the transmitter and receiver. The radio functioned with no dropped packets up to 10m, and performed with a small percentage of dropped packets at 15m. The 15 number of resends reinforced the wireless link so that it could easily satisfy the requirements put on it.

4.4 POWER SUPPLY TESTS

4.4.1 Voltage Regulation

A noisy or improperly functioning voltage regulator can cause an unstable system. Measurements of AC noise and DC voltages were taken for the 3.3V and 6.6V regulators in order to verify proper functionality. Figure 57 shows the noise on the 3.3V supply.
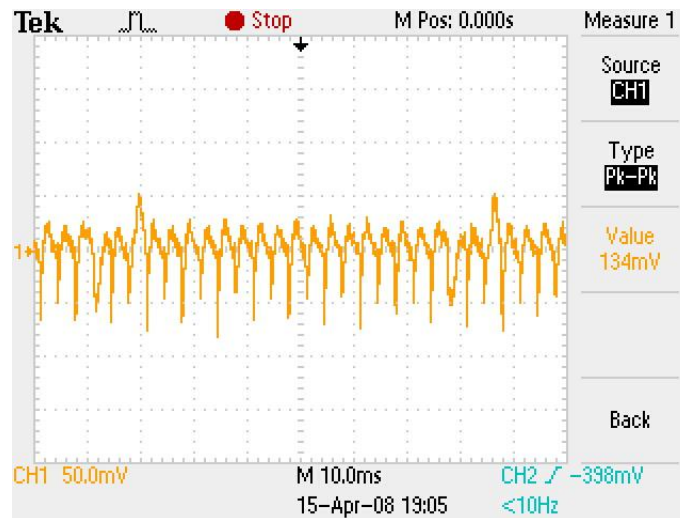
Figure 57: 3.3V Supply Noise

The 3.3V regulator's noise is mainly caused from the switching on and off of the sensor LEDs. As can be seen, voltage spikes are present every 3.3mS. This noise voltage is measured at 134mV pk-pk. This is somewhat higher than predicted, but still withing a safe margin as to

not cause problems in the system. The DC voltage is measured at 3.26V while the unit is powered, regulating properly.

Figure 58 shows the noise on the 6.6V supply.
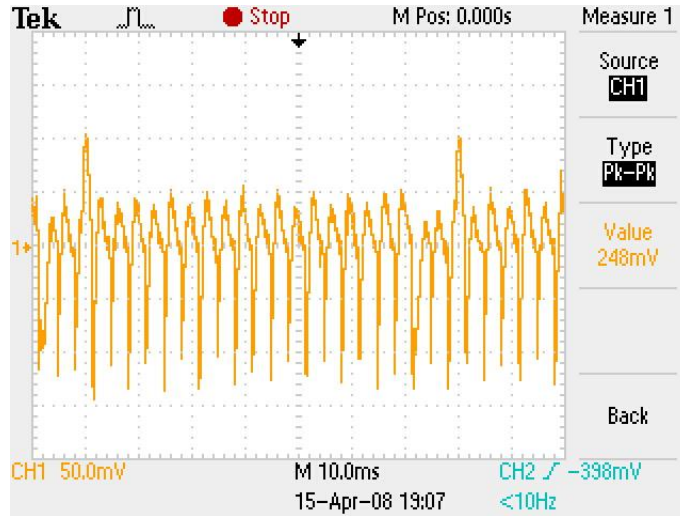
Figure 58: 6.6V Supply Noise

Similar noise spikes to those on the 3.3V regulator can be seen on the 6.6V output. Since it is a voltage doubler, the noise voltage is roughly double that of the 3.3V supply. Since this supply is only powering the LEDs and the sample-and-hold logic, this noise is at a reasonable level. The DC voltage is measured at 6.51V while the unit is powered, supply an adequate voltage.

4.4.2 Battery Life

A battery life test was planned, but due to a shortage of time, only an estimate can be provided based on current draw. The current measured from the device is 10.5mA with a 3V input. A rough approximation of battery life can be made by dividing the capacity of the battery in mAh by the battery current. Assuming a typical alkaline AA battery has 1500mAh, the battery life is about 143 hours. High capacity alkaline batteries can easily have 2500mAh. With this type of battery, the battery life is about 238 hours. Lasting longer than a week continuously running is a good clinical feature, as nurse's can replace batteries on a simple schedule.

4.5 FINAL PROTOTYPE

Two rugged, final sensor/transmitter prototypes were made for final product verification.
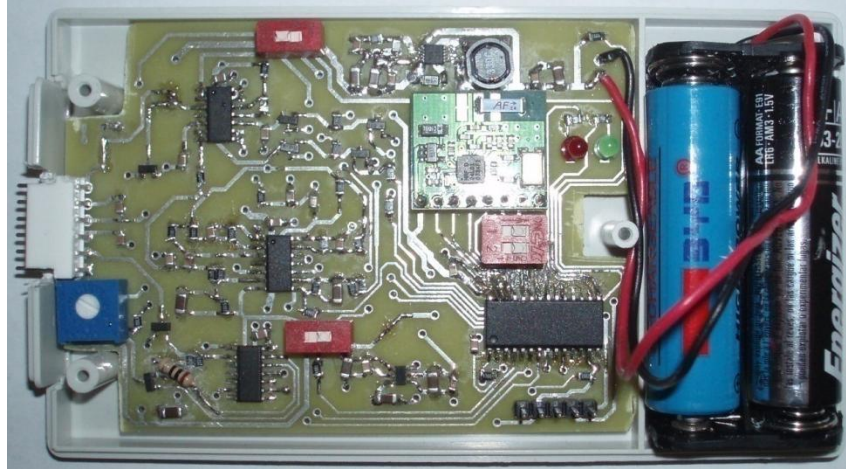
Figure 59: Final Sensor/Transmitter Prototype

A two layer PCB was designed so that the entire sensor would fit inside of a small plastic enclosure. A smaller board would have been possible using a four layer board, but that would be more expensive. Considering that one of our main objectives is a cost effective design, a larger (2.5"x3.8"), two layer board was used. Smaller parts could have been used, but at this time, easy production is most important. The top layer was used to fit all of the components, with the exception of a few bypass capacitors. It was also used for most of the signal routing.
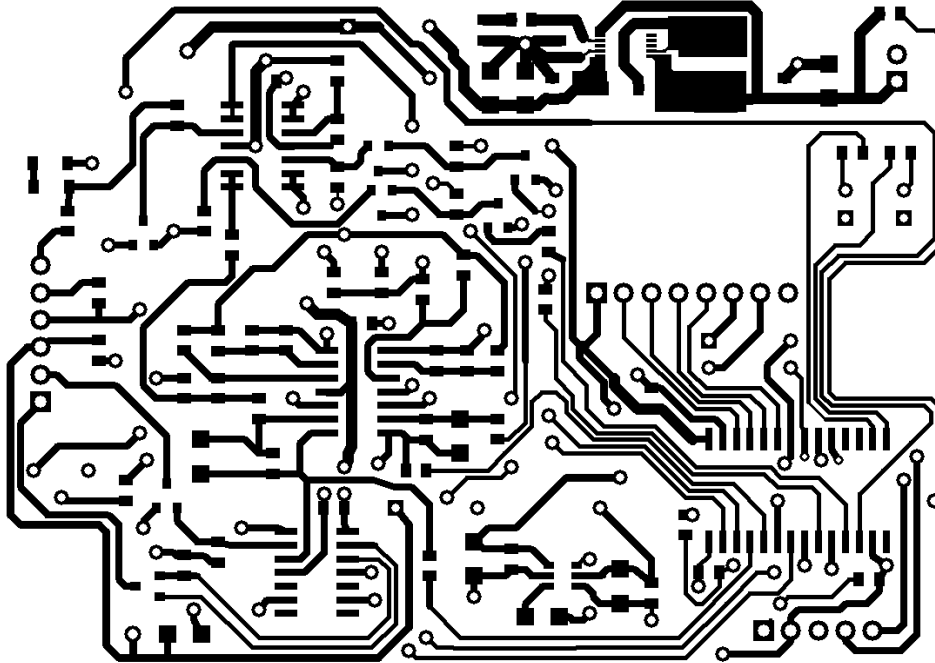
Figure 60: Top Layer of PCB

The bottom layer was used as a ground plane primarily and to route signals secondarily. Using a ground plane instead of individual traces to connect ground lowers the ground impedance significantly, resulting in lower noise and EMI. The majority of the bottom layer is a large ground plane, with vias being used to route signals between the top and bottom layers.

A final receiver prototype was made using simple through hole packages and a standard board.
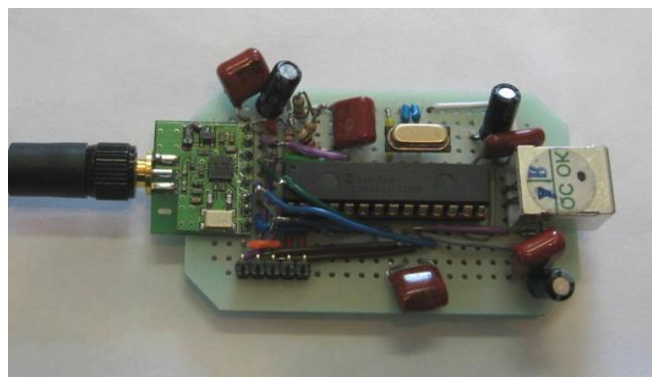
Figure 61: Final Prototype of Receiver

4.5.1 Final Prototype Testing

The final prototype was tested using an application on the PC written in Visual C++. This application displayed the patient information recorded from the the whole system. A screen shot of the application can be seen below.
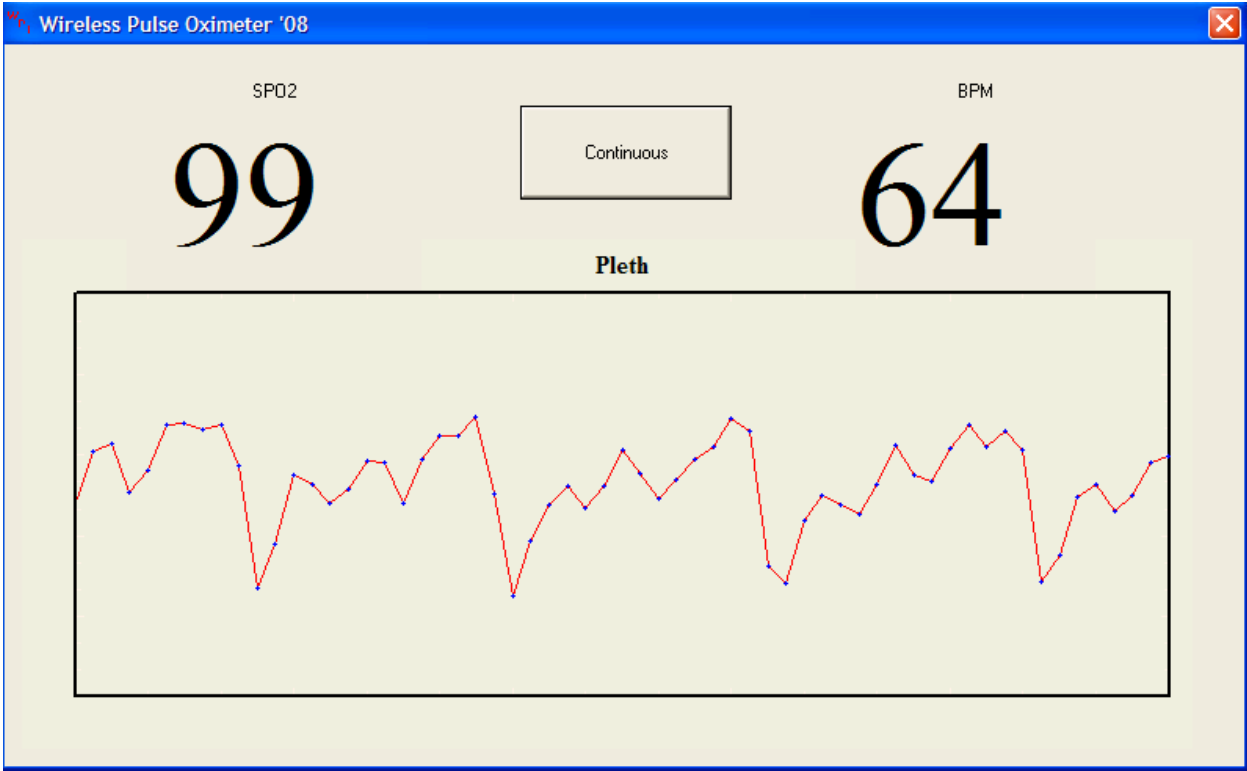
Figure 62: Screen Shot of PC Monitoring Application

5 FURTHER POSSIBLE IMPROVEMENTS

5.1 ANALOG SENSOR

In order for a pulse oximeter to be mass produced and sold, a number of things need to be completed and improved upon.

The red LED is an especially sensitive part in regards to unit-to-unit variation in specifications. In a commercial product, the red LED peak wavelength needs to me measured to within 1-2nm. This wavelength then needs to be encoded somewhere on the sensor. The most common way of doing this is via a coding resistor.

Far more testing needs to be done in order to verify the accuracy of not only the sensor, but the entire system. This testing is not only a good idea, but necessary in order to get approval by the FDA and other necessary certifications.

Improvements to the physical sensor can also be made. The current prototype is mounted on a wooden clothes pin. A flexible rubber sensor would be a good improvement. Also, the input connector from the sensor to the transmitter board needs safeguards against placing the connector on wrong. ESD protection would also be a good idea on all input connections.

5.2 DSP

A few improvements can be made to the digital signal processing portion of this project. Improvements include efficiency optimization, algorithm optimization, and additional filtering for currently-unfiltered artifacts and noise.

For efficiency optimization, a fixed-point FFT can be used on this fixed-point 16-bit PIC microcontroller. In the actual project implementation, a floating-point FFT is used, where the microcontroller uses software emulation for floating-point math which consequently used extra clock cycles. Other efficiency optimizations can include writing this fixed-point FFT and the filtering and decimation process in assembly while manually optimizing code. This would reduce duty cycle, execution time, and power consumption which would increase the device's battery life.

The beats per minute calculation is primary based on the 15 Hertz signal, which consequently increases the frequency difference between single point difference when calculating the number of points between zero-crossings. The current system uses averaging in order to compensate for this as much as possible, however the result can still tend to be slightly inaccurate during certain situations. Although more power consuming, the system could implement a calculation on a 150 Hertz signal that would be at least 10 times more accurate. A balance between a better algorithm and a higher sampled frequency while maintaining battery life could be found.

Finally, additional algorithms could be included to remove noise from additional sources. For example, the artifact of patient motion or tremoring can and does affect the pulsatile signal as it is read from the red and infrared signals. This motion does not affect the SpO2 calculation, however it greatly affects the BPM calculation. In order to remove this, an adaptive filter can be implemented with a look-up table to remove these types of artifacts.

5.3 POSSIBLE RADIO IMPROVEMENTS

The wireless link developed in this project is entirely sufficient for the requirements set forth. However, reliability is a characteristic that can always be improved, and provided a stable and robust wireless connection for this project is very important. A few techniques can be developed and used with minimal hardware changes to increase the performance of the radio link significantly. The methods described here weren't implemented in the final design due to time restrictions, but are very applicable to future design improvements.

Frequency-hopping technology is very applicable to this design. This technique takes advantage of the fact that the dangerous interference in the 2.4GHz band, for this design, is the spread-spectrum interference created by 802.11x wireless LAN systems. Below is a diagram illustrating the frequency footprints of these systems:

Figure 63: 802.11 WLAN interference bands in the 2.4GHZ channel

A convenient way to avoid the interference caused by WLAN systems is to move the operating frequency of our device away from the WLAN interference. This would usually be done using a look-up table to match the next frequency hop. Also, the frequency hops are coordinated by the master node (or base station), which avoids potential timing offsets between TX/RX pairs that end up on unmatched frequency channels[32].

A second useful technique that could be applied to improve the quality of the radio link in this system is to develop a more complex, multi-directional "cluster-tree" type sensor network. Although the software needed for such a network is quite complex, when compared to traditional "star" type network topologies, it certainly increases the range of the sensor network, and also allows potentially more sensor nodes to be connected to a single computer, enabling the remote monitoring of a greater number of patients from a single computer/base station unit.

5.4 POWER SUPPLY

Due to the large scope of the project, the power supply did not get a lot of attention. More thorough testing would be necessary, including stability, efficiency, and EMI testing. Also, a battery life remaining estimate could easily be added to the patient display. The A/D converter on the microcontroller could be used to monitor the batter voltage, and estimate the current draw from the battery based on how bright the LEDs are being driven. The brightness is monitored easily from the LED drive circuitry.

REFERENCES

---

[1] L. M. Schnapp, "Pulse Oximetry: Uses and Abuses," *Chest*, 1990, volume 98, pgs 1244-1250. Available Chestjournal.com, http://www.chestjournal.org/cgi/reprint/98/5/1244. [Accessed September 2, 2007]

[2] N. Netzer, "Overnight Pulse Oximetry for Sleep-Disordered Breathing in Adults: A Review," *Chest*, 2001, volume 120, pgs 625-633. Available Chestjournal.com, http://www.chestjournal.org/cgi/reprint/120/2/625. [Accessed September 8, 2007].

[3] C. Zamarron, "Utility of Oxygen Saturation and Heart Rate Spectral Analysis Obtained from Pulse Oximetric Recording in the Diagnosis of Sleep Apnea Syndrome," *Chest*, 2003, volume 123, pgs 1567-1576. Available Chestjournal.com, http://www.chestjournal.org/cgi/reprint/123/5/1567. [Accessed September 15, 2007].

[4] http://www.nonin.com/documents/Avant%209700%20Brochure.pdf

[5] http://www.gehealthcare.com/usen/oximetry/docs/TruSat%20Brochure.pdf

[6] http://www.nonin.com/documents/Avant%204000%20Brochure.pdf

[7] http://www.nonin.com/documents/3100%20WristOx%20Brochure.pdf

[8] http://www.spomedical.com/7500.php

[9] http://www.cambridgeconsultants.com/ws_q_med_telemetry.shtml

[10] http://www.medical.philips.com/main/products/patient_monitoring/products/philips_info_center/

[11] http://library.wpi.edu/cgi-bin/Pwebrecon.cgi?BBID=261831,
http://library.wpi.edu/cgi-bin/Pwebrecon.cgi?BBID=242297

[12] "The application of mobile computing and technology to health care services", Khawar Hameed, 2003.

[13] http://www.freepatentsonline.com/5458124.html

[14] http://www.nonin.com/about.asp?sec=1&PageID=1050

[15] http://www.vetspecs.com/images/vsm7_m_w536_h400.gif

[16] http://nonin.com/productsList.asp?PageID=2000&sec=1&sub=0

[17] http://www.jacobsschool.ucsd.edu/news/news_releases/release.sfe?id=321

[18] http://alivetec.com/images/pulseoxhand.jpg, http://alivetec.com/products.htm

[19] http://www.freescale.com/files/rf_if/doc/data_sheet/MC13202.pdf

[20] Principles of Wireless Networks, pg508, K. Pahlavan, P. Krishnamurphy.

[21] http://en.wikipedia.org/wiki/ZigBee, http://plato.csie.ncku.edu.tw/Network-slides-dir/ZigbeeWireless-Craig.pdf

[22] http://en.wikipedia.org/wiki/ZigBee, http://plato.csie.ncku.edu.tw/Network-slides-dir/ZigbeeWireless-Craig.pdf

[23] http://en.wikipedia.org/wiki/ZigBee

[24] J. G. Webster, et al, *Design of Pulse Oximeters*, Series in Medical Physics and Biomedical Engineering. Boca Raton: CRC Press, 1997.

[25] Yitzhak Mendelson, "Pulse Oximetry", in Wiley Encyclopedia of Biomedical Engineering, John Wiley & Sons, Inc, 2006.

[26] Pulse Oximetry: Principles and Limitations; James E. Sinex, MD

[27] http://www.analog.com/library/analogdialogue/archives/41-01/pulse_oximeter.html

[28] Design of Pulse Oximeters, Oliver Wieben

[29] http://ieeexplore.ieee.org/iel2/691/6333/00247420.pdf?tp=&isnumber=&arnumber=247420

[30] http://en.wikipedia.org/wiki/Free_space_loss

[31] http://www.sparkfun.com/datasheets/Wireless/Antenna/DA-24-04.pdf

[32] http://www.nordicsemi.no/files/Product/applications/Frequency_Agility_Protocol_for_nRF24XX.pdf

APPENDIX A
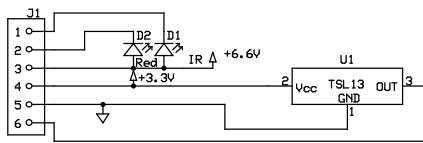
WP0X08		
Finger Sensor		
Joseph Bailey	Rev 1.0	Page #1
	3/14/2008	
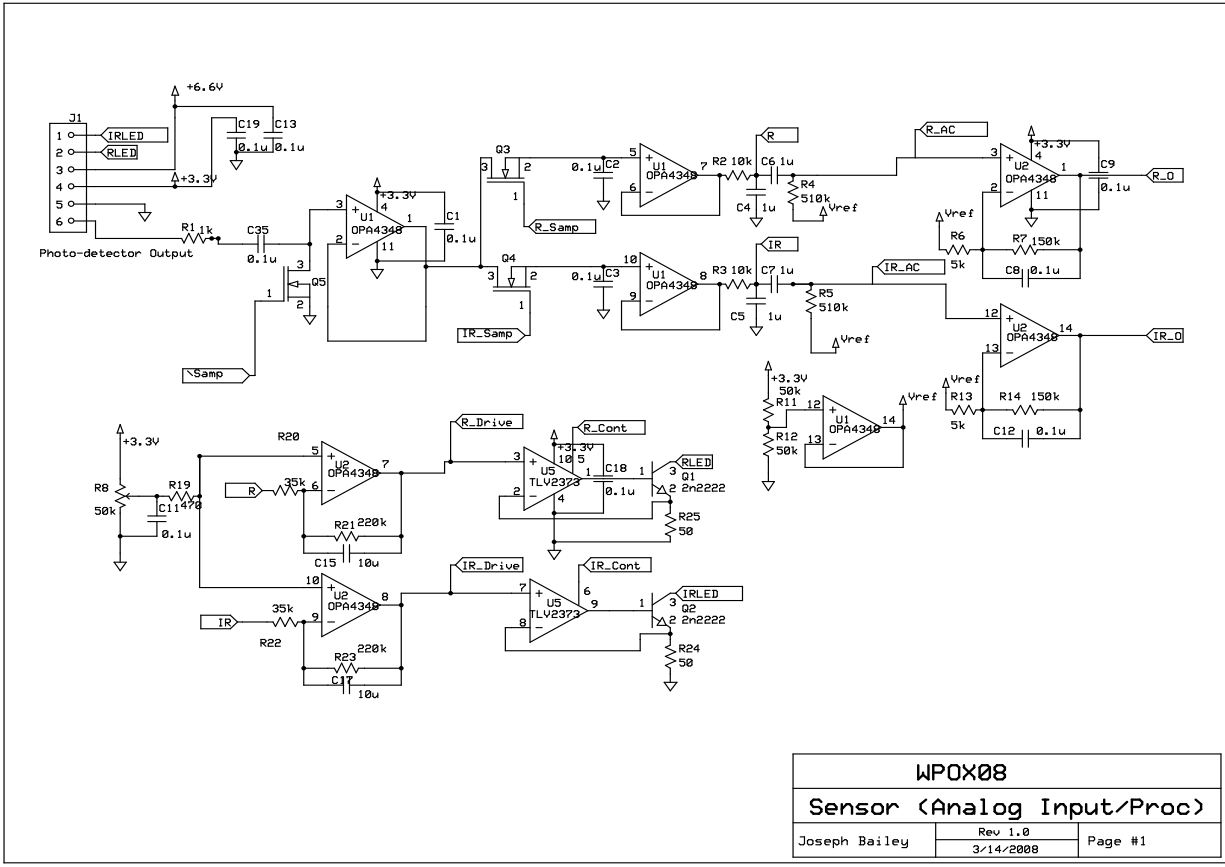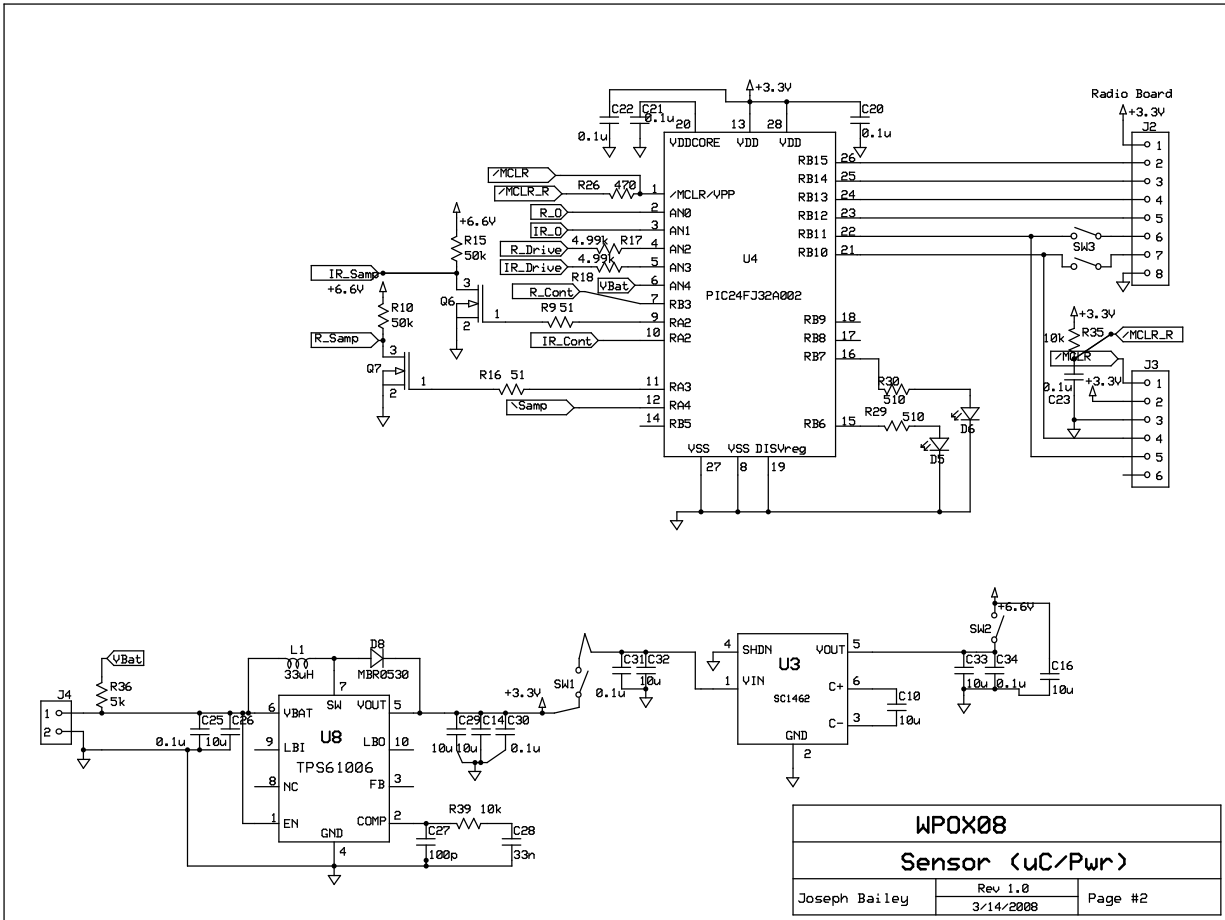
WP0X08

Sensor (uC/Pwr)

Joseph Bailey	Rev 1.0	Page #2
	3/14/2008	

Programming Port

J3

1 — >MCLR
2 — +5v
3
4 — PGD
5 — PGC
6

+5v

U
20 VDD

RA0/AN0   RB0/SDA 21 — <MISO
RA1/AN1   RB1/SCL 22 — <SCL
RA2/AN2   RB2/VMO 23
RA3/AN3   RB3/VPO 24
RA4/T0CKI RB4/KBI0 25 — <IRQ
RA5/AN4   RB5/PGM 26
           RB6/PGC 27 — <PGC
           RB7/PGD 28 — <PGD
PIC18F2550
OSC1/CLKI RC0/T1OSO 11
OSC2/CLKO RC1/T1OSI 12
/MCLR/VPP RC2/CCP1 13
           VUSB   14
           RC4/D-   15
           RC5/D+   16
           RC6/TX   17
           RC7/RX   18 — <MOSI

VSS VSS
8   19

CSN
CE

R3 10k +5v
R2 10k +5v

C1 15pF
C2 15pF
X1 20MHz
R1 470
C5 0.1u
>MCLR

Radio Board

+5v   J2
1
CE   2
CSN   3
SCL   4   C4
MOSI   5   1u
MISO   6
IRQ   7
8

USB

+5v   J1
1
2   C3   C6
3   10u 0.1u
4

WPOX08
Receiver
Noah Pendleton Rev 1.0   Page # 1
                4/02/2008

APPENDIX B

QTY	Ref.	Value	Description	Dist.	Part No.	MFG Part No.	Unit	Sub.
Wireless Pulse Oximeter Bill of Materials						MQP HH MQP1	(All Costs per 1000 units)	
Patient Worn Device								
22	C1-C5;C8;C9;C11-C13;C18-C25;C30;C31;C34;C35	0.1u	805 ceramic chip capacitor	Mouser	80-C0805C104K5R	C0805C104K5RACTU	0.012	0.264
2	C6;C7	1u	805 ceramic chip capacitor	Mouser	80-C0805C105K4P	C0805C105K4PACTU	0.03	0.06
9	C26;C33;C15;C17;C32;C14;C16;C29;C10	10u	1206 ceramic chip capacitor	Mouser	80-C1206C106K4P	C1206C106K4PACTU	0.1	0.9
1	C27	100p	805 ceramic chip capacitor	Mouser	80-C0805C101K5G	C0805C101K5RACTU	0.011	0.011
1	C28	33n	805 ceramic chip capacitor	Mouser	80-C0805C333K5R	C0805C333K5RACTU	0.016	0.016
2	D1;D2	1N4148	Gen Purpose Diode	Mouser	512-MMBD4148	MMBD4148	0.019	0.038
1	D5		Red/Green LED	Mouser	604-AM23ESGC	AM23ESGC	0.2	0.2
2	D7;D8		Schottkey Diode	Mouser	512-MBR0530	MBR0530	0.048	0.096
1	J1		6 Pin Rt. Angle Header	Mouser	571-6404556	640455-6	0.161	0.161
1	J2		2.4GHz Radio Board	SparkFun			23.96	23.96
1	J3		5 Pin Header (Program Port)	Mouser	538-22-28-4050	22-28-4050	0.15	0.15
1	J4		2 Pin Header for Battery	Mouser	571-6404572	640457-2	0.166	0.166
1	L1	24S330C	Low Resistance Inductor	Mouser	580-24S330C	24S330C	0.5	0.5
2	Q1;Q2	2N2222	NPN Transistor	Mouser	512-MMBT2222	MMBT2222	0.022	0.044
5	Q3-Q7	2N7002	N Channel MOSFET	Mouser	512-2N7002	2N7002	0.038	0.19
1	R1	1k	805 chip resistor	Mouser	71-CRCW0805-1.0K-E3	CRCW08051K00FKEA	0.01	0.01
7	R2;R3;R6;R13;R27;R35;R39	10k	805 chip resistor	Mouser	71-CRCW0805-10K-E3	CRCW080510K0FKEA	0.01	0.07
2	R4;R5	510k	805 chip resistor	Mouser	71-CRCW0805-510K-E	CRCW0805510KFKEA	0.01	0.02
2	R7;R14	150k	805 chip resistor	Mouser	71-CRCW0805-150K-E	CRCW0805150KFKEA	0.01	0.02
4	R10;R11;R12;R15	51k	805 chip resistor	Mouser	71-CRCW080551K0FKI	CRCW080551K0FKEA	0.01	0.04
4	R19;R26;R29;R30	470	805 chip resistor	Mouser	71-CRCW0805-470-E3	CRCW0805470RFKEA	0.01	0.04
2	R20;R22	36k	805 chip resistor	Mouser	71-CRCW080536K0FKI	CRCW080536K0FKEA	0.01	0.02
2	R21;R23	220k	805 chip resistor	Mouser	71-CRCW0805220KFKI	CRCW0805220KFKEA	0.01	0.02
4	R9;R16R24;R25	51	805 chip resistor	Mouser	71-CRCW080551R0FKI	CRCW080551R0FKEA	0.01	0.04
3	R17;R18;R36	4.99k	805 chip resistor	Mouser	71-CRCW0805-4.99K-E	CRCW08054K99FKEA	0.01	0.03
1	R8	50k	Potentiometer	Mouser	652-3386P-1-503LF	3386P-1-503LF	0.68	0.68
2	~~SW1;SW2~~	(Only Used in Prototype)	~~1POS SPST DIP SW~~	Mouser	~~611-BD01~~	~~BD01~~		0
1	~~SW3~~	(Only Used in Prototype)	~~2POS SPST DIP SW~~	Mouser	~~611-BD02~~	~~BD02~~		0
2	U1;U2	OPA4348	Quad uPwr Opamp	Mouser	595-OPA4348AID	OPA4348AID	0.676	1.352
1	U5	TLV2373	Dual uPwr Opamp	Mouser	595-TLV2373ID	TLV2373ID	0.741	0.741
1	U4	PIC24FJ32A002	16-bit uController	Mouser	579-PIC24FJ32GA02SC	PIC24FJ32GA002-I/SO	2	2
1	U8	TPS61006	3.3V Step-Up Regulator	Mouser	595-TPS61006DGS	TPS61006DGS	1.17	1.17
1	U3	SC1462	Charge Pump Regulator	Mouser	SC1462ISKCT-ND	SC1462ISKTRT	0.6875	0.6875
Sensor								
			6 Pin Connector	Mouser	571-3-640442-6	3-640442-6	0.159	0
1	U1	TSL12S	Photodector	Mouser	856-TSL12S-LF	TSL12S-LF	1.26	1.26
1	D2	LTL-4266N	Red LED	Mouser	859-LTL-4266N	LTL-4266N	0.22	0.22
1	D1	QEC113	IR LED	Mouser	512-QEC113	QEC113	0.19	0.19
				Mouser				
Receiver				Mouser				
1	R1	470	805 chip resistor	Mouser	71-CRCW0805-470-E3	CRCW0805470RFKEA	0.01	0.01
2	R2;R3	10k	805 chip resistor	Mouser	71-CRCW0805-10K-E3	CRCW080510K0FKEA	0.01	0.02
2	C6;C5	0.1u	805 ceramic chip capacitor	Mouser	80-C0805C104K5R	C0805C104K5RACTU	0.012	0.024
1	C3	10u	1206 ceramic chip capacitor	Mouser	80-C1206C106K4P	C1206C106K4PACTU	0.1	0.1
1	C4	1u	805 ceramic chip capacitor	Mouser	80-C0805C105K4P	C0805C105K4PACTU	0.03	0.03
2	C1;C2	15pF	capacitor	Mouser	80-C0805C150K1G	C0805C150K1GACTU	0.088	0.176
1	U1	PIC18F2550	USB Microcontroller	Mouser	579-PIC18F2550-I/SP	PIC18F2550-I/SP	3.5	3.5
1	J1		USB Type B Connector	Mouser	806-KUSBX-BS1N-B	KUSBX-BS1N-B	0.38	0.38
1	J2		2.4GHz Radio Board	SparkFun			23.96	23.96
1	J3		5 Pin Header (Program Port)	Mouser	538-22-28-4050	22-28-4050	0.15	0.15
1	X1	20MHz	Crystal	Mouser	520-HCU2000-SX	ECS-200-S-4X 20.0	0.37	0.37
Case Assembly								
1	NA	1117	Enclosure	Mouser	546-001117		1117	6	6
Total Parts:							Total Cost:	
108								70.0865

APPENDIX C

FFT Reference Code

```
for(s=1;s<=q;s++) {
N_Hat = 1<<s;
      B=N/N_Hat;
      for(b=0;b<B;b++) {
            l = b*N_Hat;
            for(o=0;o<N_Hat/2;o++) {

                  //FFT for Red LED data
                  temp2r    =    Wr[B*o]*xREALred[cbi][l+o+N_Hat/2]    -
Wi[B*o]*xIMAGred[cbi][l+o+N_Hat/2];
                  temp2i    =    Wi[B*o]*xREALred[cbi][l+o+N_Hat/2]    +
Wr[B*o]*xIMAGred[cbi][l+o+N_Hat/2];
                  t1r = xREALred[cbi][l+o]+temp2r;
                  t1i = xIMAGred[cbi][l+o]+temp2i;
                  t2r = xREALred[cbi][l+o]-temp2r;
                  t2i = xIMAGred[cbi][l+o]-temp2i;
                  xREALred[cbi][l+o]=t1r;
                  xIMAGred[cbi][l+o]=t1i;
                  xREALred[cbi][l+o+N_Hat/2]=t2r;
                  xIMAGred[cbi][l+o+N_Hat/2]=t2i;

                  //FFT for IR LED data
                  temp2r    =    Wr[B*o]*xREALir[cbi][l+o+N_Hat/2]    -
Wi[B*o]*xIMAGir[cbi][l+o+N_Hat/2];
                  temp2i    =    Wi[B*o]*xREALir[cbi][l+o+N_Hat/2]    +
Wr[B*o]*xIMAGir[cbi][l+o+N_Hat/2];
                  t1r = xREALir[cbi][l+o]+temp2r;
                  t1i = xIMAGir[cbi][l+o]+temp2i;
                  t2r = xREALir[cbi][l+o]-temp2r;
                  t2i = xIMAGir[cbi][l+o]-temp2i;
                  xREALir[cbi][l+o]=t1r;
                  xIMAGir[cbi][l+o]=t1i;
```

```
                    xREALir[cbi][l+o+N_Hat/2]=t2r;

                    xIMAGir[cbi][l+o+N_Hat/2]=t2i;

              }

       }

}


for(k=0;k<N;k++) {

       mag[0][k]        =         sqrt((xREALred[cbi][k]*xREALred[cbi][k])        +
(xIMAGred[cbi][k]*xIMAGred[cbi][k]));

       mag[1][k]        =         sqrt((xREALir[cbi][k]*xREALir[cbi][k])        +
(xIMAGir[cbi][k]*xIMAGir[cbi][k]));
```

APPENDIX D

Datasheet References

http://focus.ti.com/lit/ds/symlink/cc2500.pdf

http://www.atmel.com/dyn/resources/prod_documents/doc4779.pdf

http://www.nordicsemi.com/files/Product/data_sheet/nRF24L01_Product_Specification_v2_0.pdf

http://ww1.microchip.com/downloads/en/DeviceDoc/39881c.pdf

http://ww1.microchip.com/downloads/en/devicedoc/39632c.pdf